Electronic Supplementary Material (ESI) for Physical Chemistry Chemical Physics.
This journal is © the Owner Societies 2023

Electronic Supplementary Information for:

Effect of Thionation of Carbonyl Group on the Photophysics of Compact Spiro Rhodamine-Naphthalimide Electron Donor-Acceptor Dyads: Intersystem Crossing, Charge Separation and Electron Spin Dynamics

Xiao Xiao,[a‡] Tong Mu,[b‡] Andrey A. Sukhanov,[b‡] Yihang Zhou,[a] Peiran Yu,[a] Fabiao Yu,[c] Ayhan Elmali,[d] Jianzhang Zhao,*[a] Ahmet Karatay*[d] and Violeta K. Voronkova*[b]

[a] State Key Laboratory of Fine Chemicals, Frontier Science Center for Smart Materials, School of Chemical Engineering, Dalian University of Technology, 2 Ling Gong Rd., Dalian 116024, P. R. China. *E-mail: zhaojzh@dlut.edu.cn (J. Z.)

[b] Zavoisky Physical-Technical Institute FRC Kazan Scientific Center of RAS, Sibirsky Tract 10/7, Kazan 420029, Russia. *E-mail: vio@kfti.knc.ru (V. K. V.)

[c] Key Laboratory of Hainan Trauma and Disaster Rescue, The First Affiliated Hospital of Hainan Medical University, Hainan Medical University, Haikou 571199, P. R. China.

[d] Department of Engineering Physics, Faculty of Engineering, Ankara University, 06100, Ankara, Türkiye. *E-mail: akaratay@eng.ankara.edu.tr (A. K.)

‡These authors contributed equally to this work.

Index

1. General Information and Synthesis

All the chemicals used in synthesis are analytically pure and were used as received, the solvents were dried and distilled before synthesis. ^{1}H and ^{13}C NMR spectra were recorded on the Bruker Avance spectrometers (400 MHz, 500 MHz or 600 MHz). The mass spectra were measured by EI-TOF-HRMS spectrometer.

Synthesis of compound 2.[1] Under N_2 atmosphere, compound 1 (1.00 g, 5.0 mmol) and sodium dichromate (3.73 g, 14.1 mmol) were dissolved in acetic acid (17 mL). The mixture was stirred and refluxed for 6 h. After the reaction was finished, the mixture was cooled down to room temperature, and the solvent was evaporated under reduced pressure. Then cold water (30 mL) was added to the mixture and the mixture was stirred at 0 °C for 15 min. The solid precipitate was formed and then filtrated. The precipitate was washed with water until the filtrate was neutral. The solid was dried in vacuum to obtain the yellow powder (0.86 g, yield: 71%). The product was directly used for the next step without further purification.

Synthesis of compound 3.[1] Under N_2 atmosphere, *n*-butylamine (0.5 mL, 5.1 mmol) was added to the stirred solution of compound 2 (800 mg, 3.3 mmol) in ethanol (50 mL). The reaction mixture was refluxed at 80 °C for 2 h. After the reaction was finished, the mixture was cooled down to room temperature, and the solvent was evaporated under reduced pressure. Then the residue was purified with column chromatography (silica gel, DCM:PE = 3:1, v/v) to give a light yellow solid (521 mg, yield: 53%). ^{1}H NMR ($CDCl_3$, 400 MHz): δ 8.84–8.82 (m, 1H), 8.74–8.72 (m, 1H), 8.70–8.67 (m, 1H), 8.41–8.39 (m, 1H), 8.01–7.96 (m, 1H), 4.19 (t, J = 7.6 Hz, 2H), 1.77–1.69 (m, 2H), 1.50–1.41 (m, 2H), 0.99 (t, J = 7.4 Hz, 3 H).

Synthesis of compound 4.[1] Under N_2 atmosphere, Compound 3 (420 mg, 1.4 mmol) and $SnCl_2{\cdot}2H_2O$ (2.06 g, 9.1 mmol) were dissolved in ethanol (15 mL), and then hydrochloric acid (6 mL) was added into the mixture dropwise. The reaction mixture was stirred at room temperature for 0.5 h. Then, the reaction was quenched by the 10% Na_2CO_3 aqueous solution (60 mL) and filtered. The filtrate was washed with water (3 × 45 mL) to obtain the viscous orange solid. Then the solid was dissolved in the DCM (60 mL) and washed with brine solution (60 mL × 3). The organic layer was dried over the anhydrous Na_2SO_4 and the solvent was removed under reduced pressure. Then the solid was dried in vacuum to obtain

the yellow powder (360 mg, yield: 96%). The product was directly used for the next step without further purification.

Synthesis of compound NIS-NH$_2$.[2] Compound 4 (0.28 g, 1.0 mmol) and Lawesson's reagent (1.68 g, 4.2 mmol) were dissolved in dry toluene (25 mL). The mixture was stirred and refluxed for 21 h. After the reaction was finished, the mixture was cooled down to room temperature, and the solvent was evaporated under reduced pressure. The residue was purified with column chromatography (silica gel, DCM:PE = 3:2, v/v) to give a black powder (89 mg, yield: 30%). M.p.: 177.0–177.8 °C. ^{1}H NMR ($CDCl_3$, 400 MHz): δ 9.00 (d, J = 7.8 Hz, 1H), 8.85 (d, J = 8.4 Hz, 1H), 8.01 (d, J = 8.0 Hz, 1H), 7.55–7.52 (m, 1H), 6.81 (d, J = 8.4 Hz, 1H), 5.40 (s, 2H), 5.10 (s, 2H), 1.96–1.88 (m, 2H), 1.50–1.45 (m, 2H), 1.00 (t, J = 7.4 Hz, 3H). HRMS-ESI ($[C_{16}H_{16}N_2S_2 + H]^+$), *m/z*: calcd: 301.0833; found: 301.0813.

Synthesis of compound NIS-NHAc. NIS-NH$_2$ (66.7 mg, 0.25 mmol) were dissolved in acetic acid (0.5 mL) and acetic anhydride (0.5 mL). The mixture was stirred and refluxed for 12 h. After the reaction was finished, the mixture was cooled down to room temperature, and the solvent was evaporated under reduced pressure. The residue was purified with column chromatography (silica gel, DCM) to give a dark red powder (22.0 mg, yield: 26%). M.p.: 235.4–236.8 °C. ^{1}H NMR (DMSO-d_6, 400 MHz): δ 10.40 (s, 1H), 8.89 (d, J = 7.8 Hz, 1H), 8.82 (d, J = 8.6 Hz, 1H), 8.75 (d, J = 8.5 Hz, 1H), 8.33 (d, J = 8.5 Hz, 1H), 7.82 (dd, J = 7.8 Hz, 1H), 5.26 (t, J = 7.4 Hz, 2H), 2.30 (s, 3H), 1.88–1.81 (m, 2H), 1.46–1.37 (m, 2H), 0.96 (t, J = 7.4 Hz, 3H). ^{13}C NMR (DMSO-d_6, 100 MHz): δ 190.11, 189.11, 169.64, 141.09, 139.22, 138.15, 129.23, 128.59, 126.92, 124.34, 123.44, 122.94, 119.84, 54.12, 26.82, 24.20, 19.44, 13.50. HRMS-ESI ($[C_{18}H_{18}N_2OS_2 + H]^+$), *m/z*: calcd: 343.0939; found: 343.0946.

Synthesis of compound Rho.[3] Under N_2 atmosphere, RB (100 mg, 0.23 mmol) were dissolved in dry 1,2-dichloroethane (5 mL), then $POCl_3$ (0.1 mL) was added dropwise to the mixture. The reaction mixture was stirred and refluxed for 6 h. After cooling down to room temperature, the solvent was evaporated under reduced pressure. The residue was dissolved in dry acetonitrile (10 mL). Then under N_2 atmosphere, *n*-butylamine (1 mL) and Et_3N (0.3 mL) were added dropwise to the mixture at room temperature, the mixture was stirred and refluxed for 25 h. After the reaction was finished, the mixture was cooled down to room temperature, and the solvent was evaporated under reduced pressure. The crude product was purified by column chromatography (silica gel, DCM:PE = 1:1, v/v) to give a pink solid (95 mg, yield: 83%).

2. Molecular Structure Characterization Data

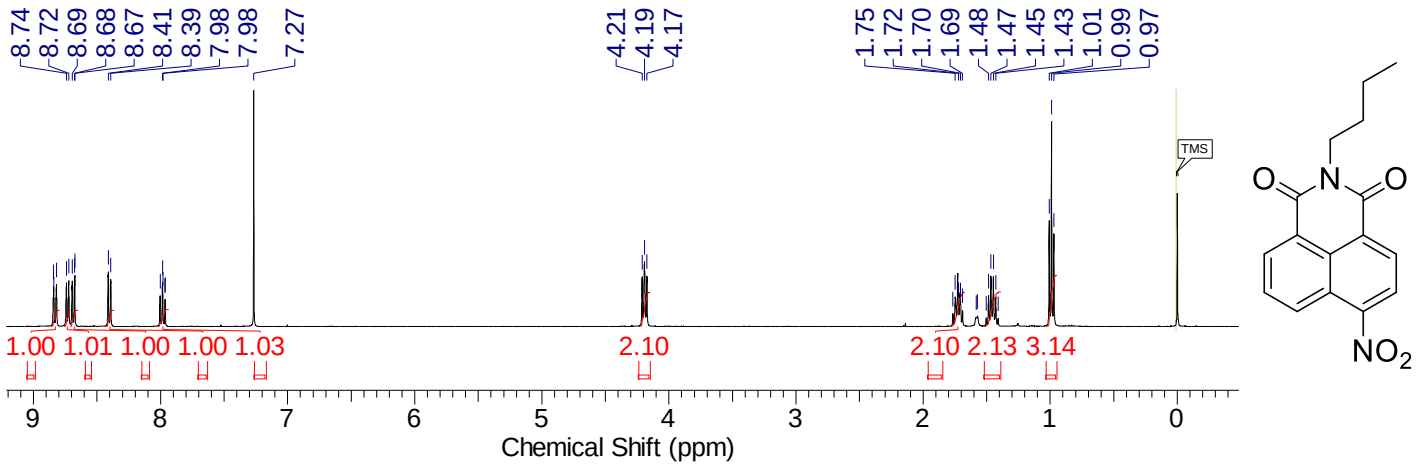

Fig. S1 ^{1}H NMR spectrum of **3** (400 MHz, $CDCl_3$).

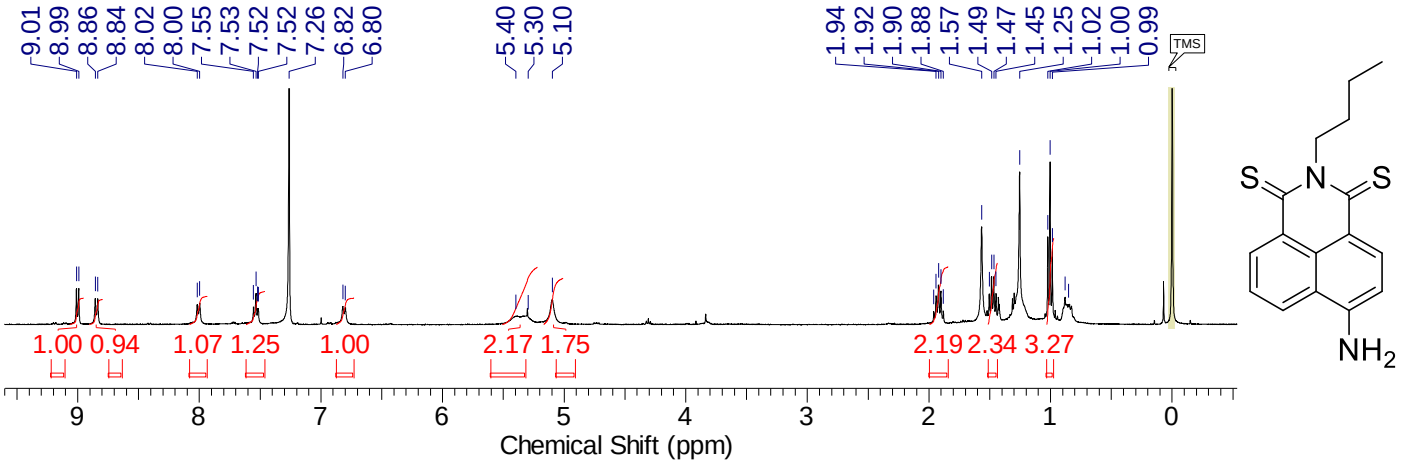

Fig. S2 ^{1}H NMR spectrum of **NIS-NH$_2$** (400 MHz, $CDCl_3$).

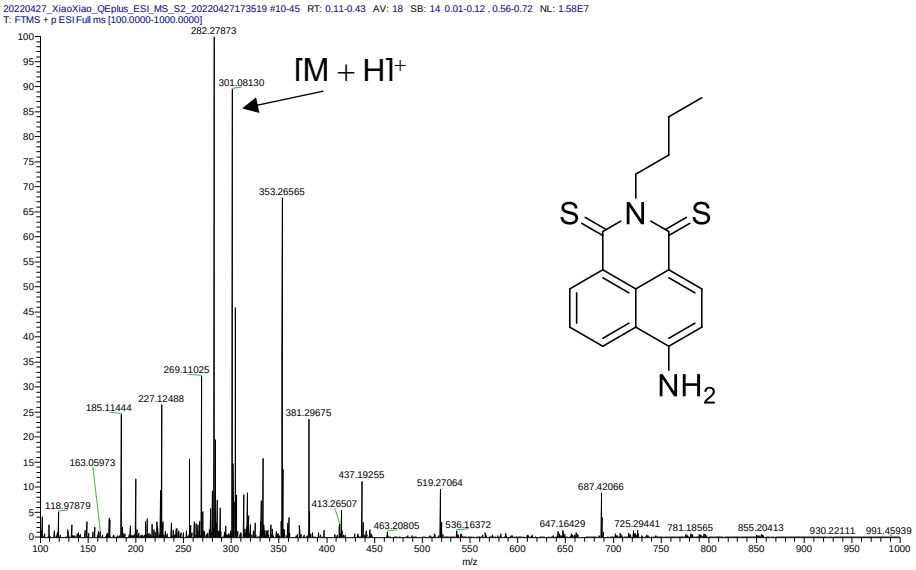

Fig. S3 ESI-HRMS of **NIS-NH$_2$**.

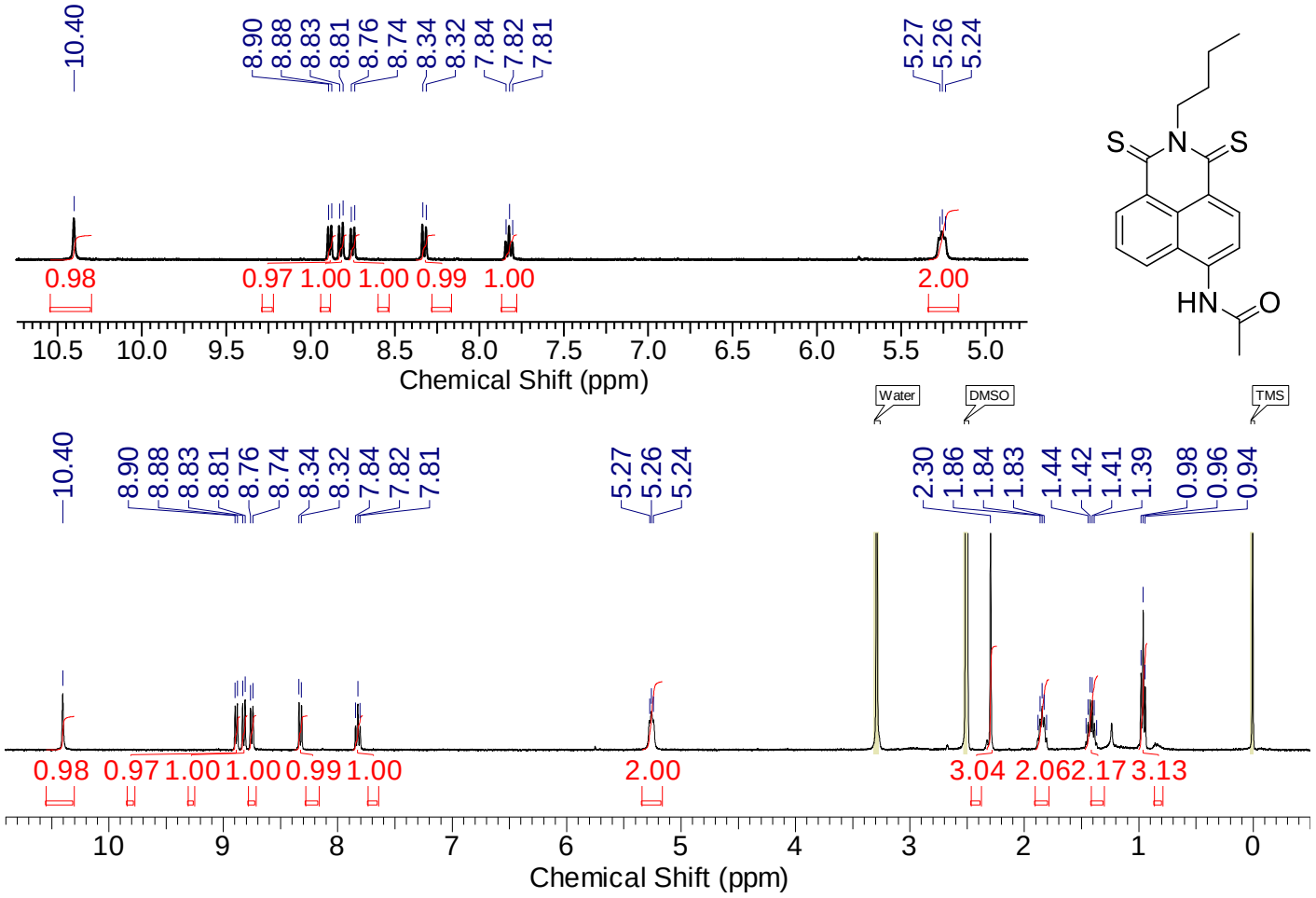

Fig. S4 ^{1}H NMR spectrum of **NIS-NHAc** (400 MHz, DMSO-d_6).

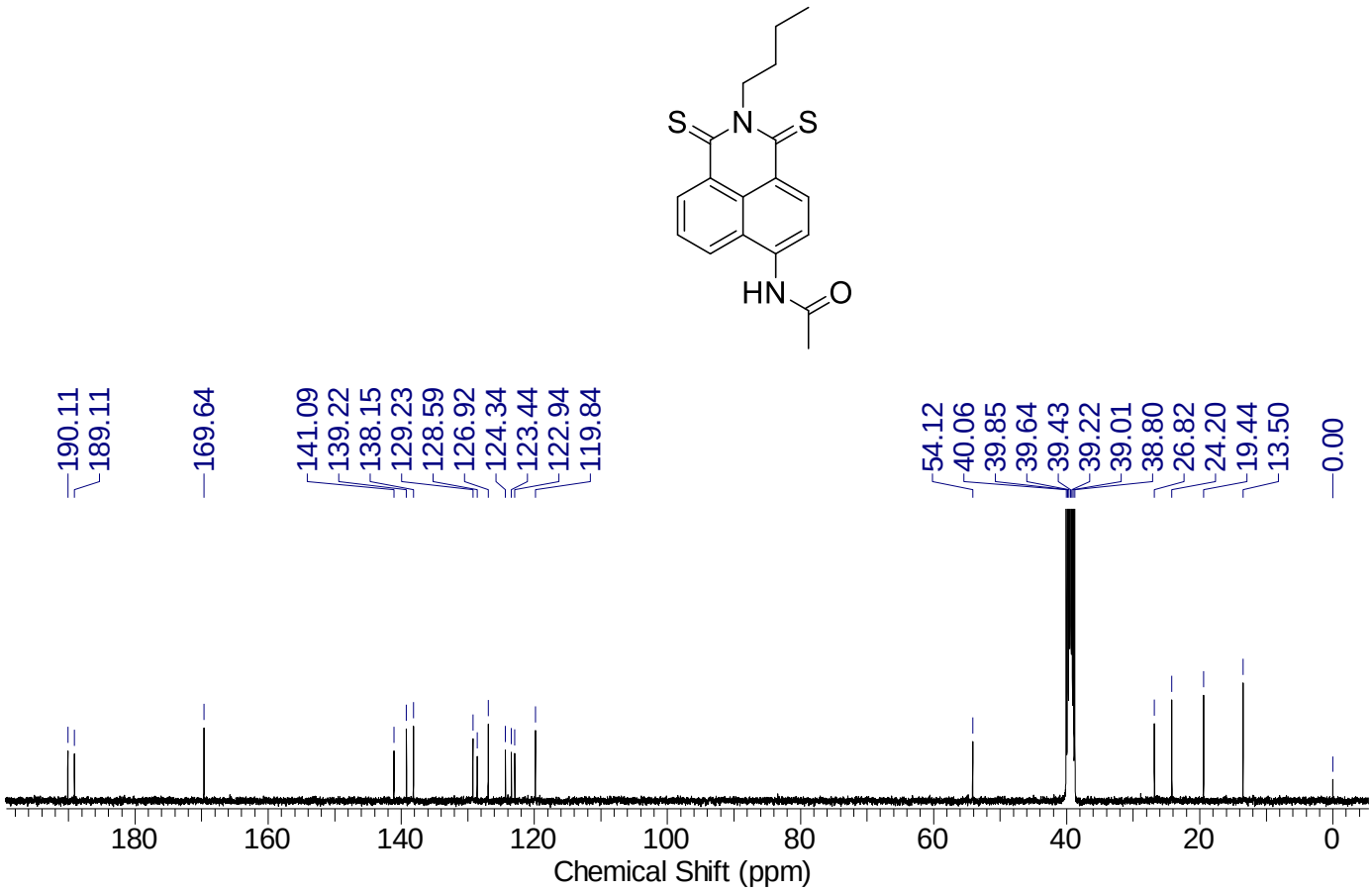

Fig. S5 ^{13}C NMR spectrum of **NIS-NHAc** (100 MHz, DMSO-d_6).

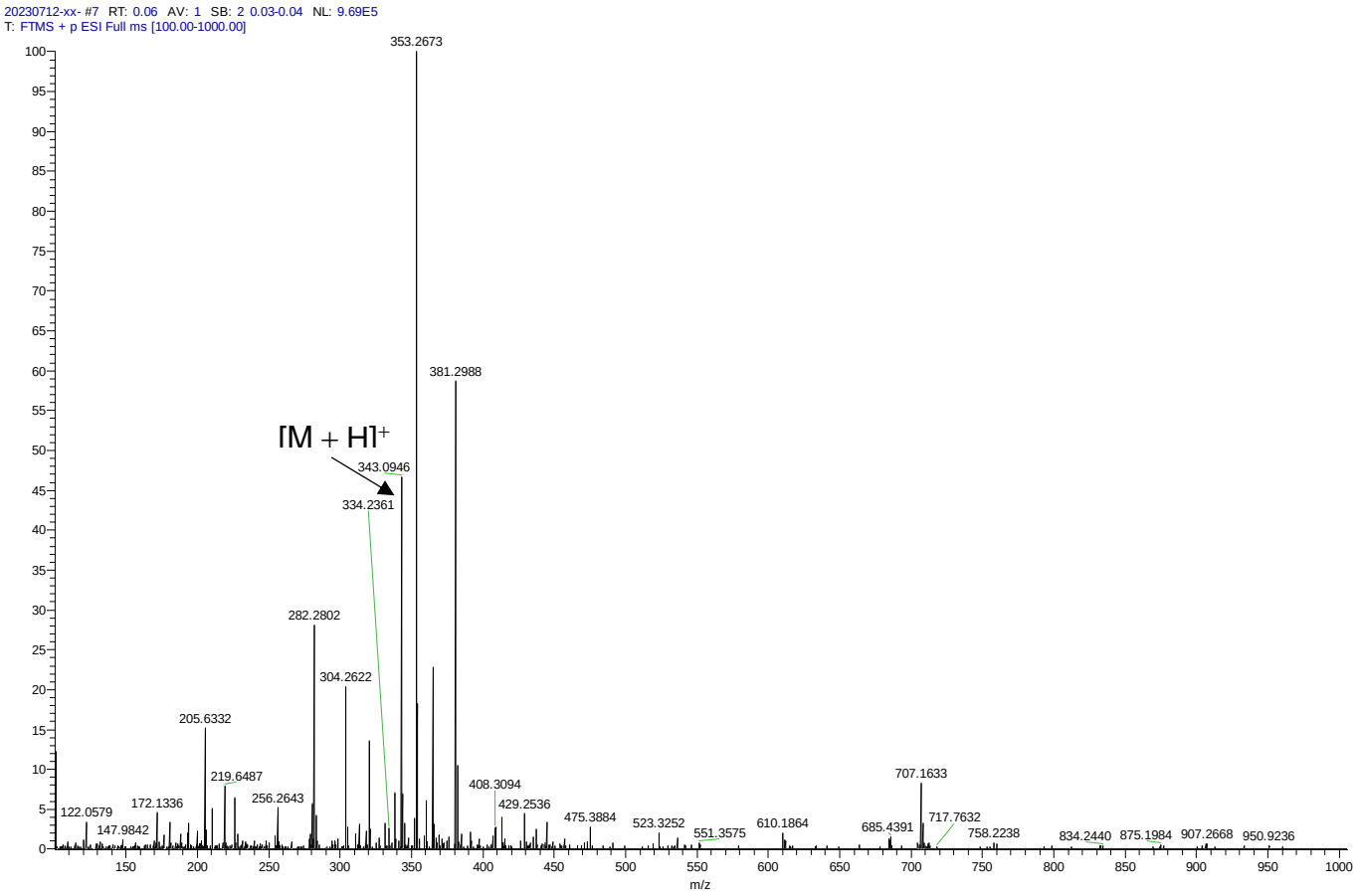

Fig. S6 ESI-HRMS of **NIS-NHAc**.

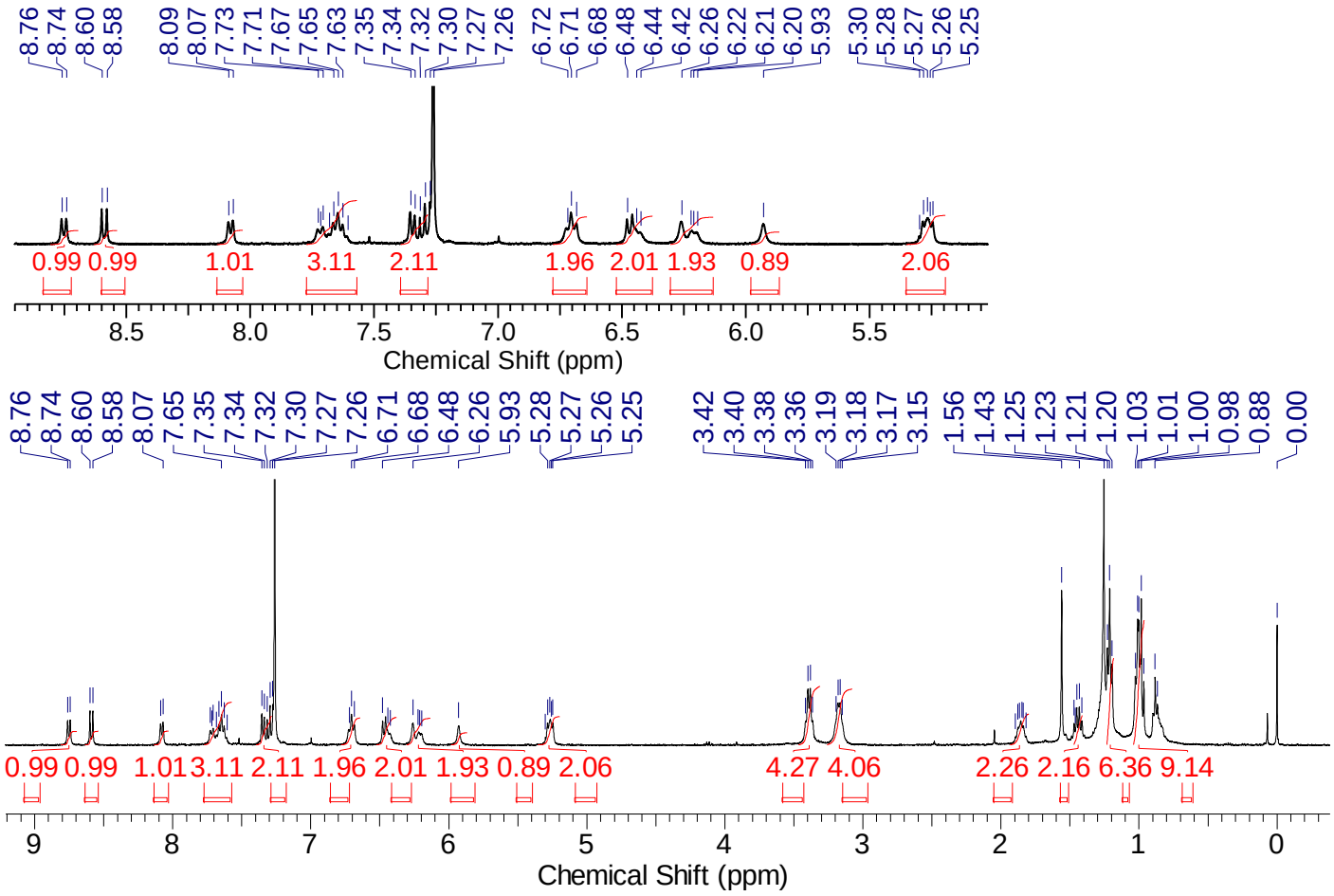

Fig. S7 ^{1}H NMR spectrum of **Rho-NIS** (400 MHz, $CDCl_3$).

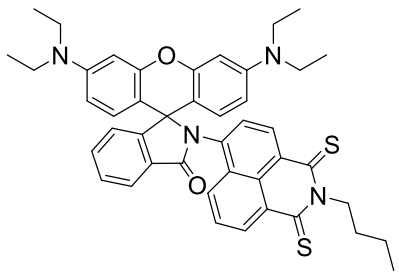

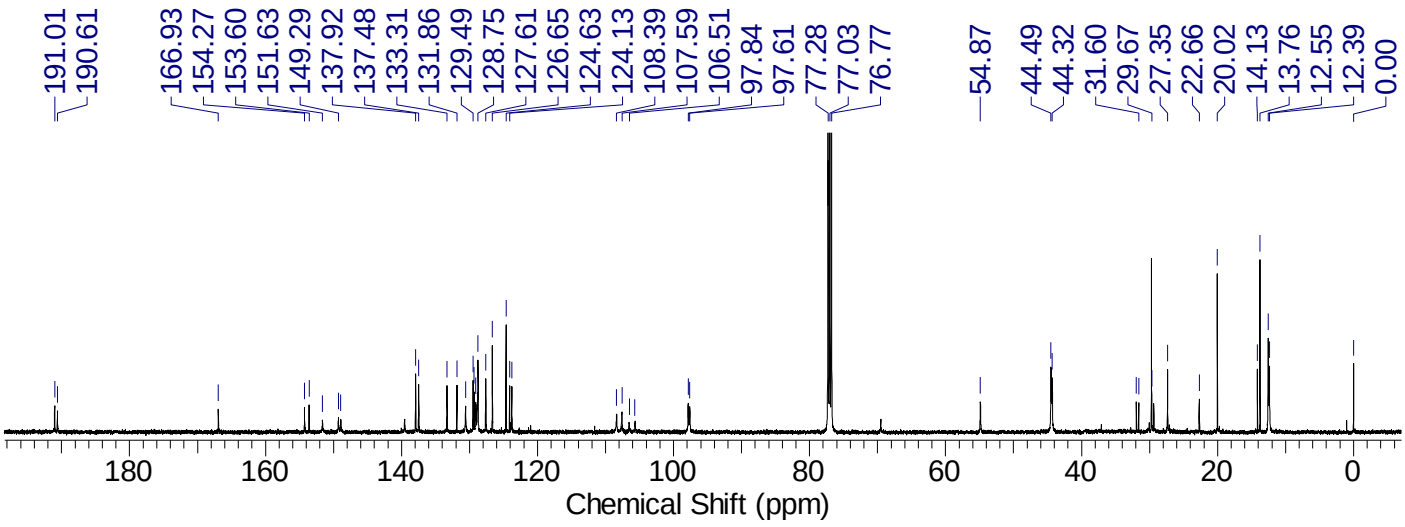

Fig. S8 ^{13}C NMR spectrum of **Rho-NIS** (125 MHz, $CDCl_3$).

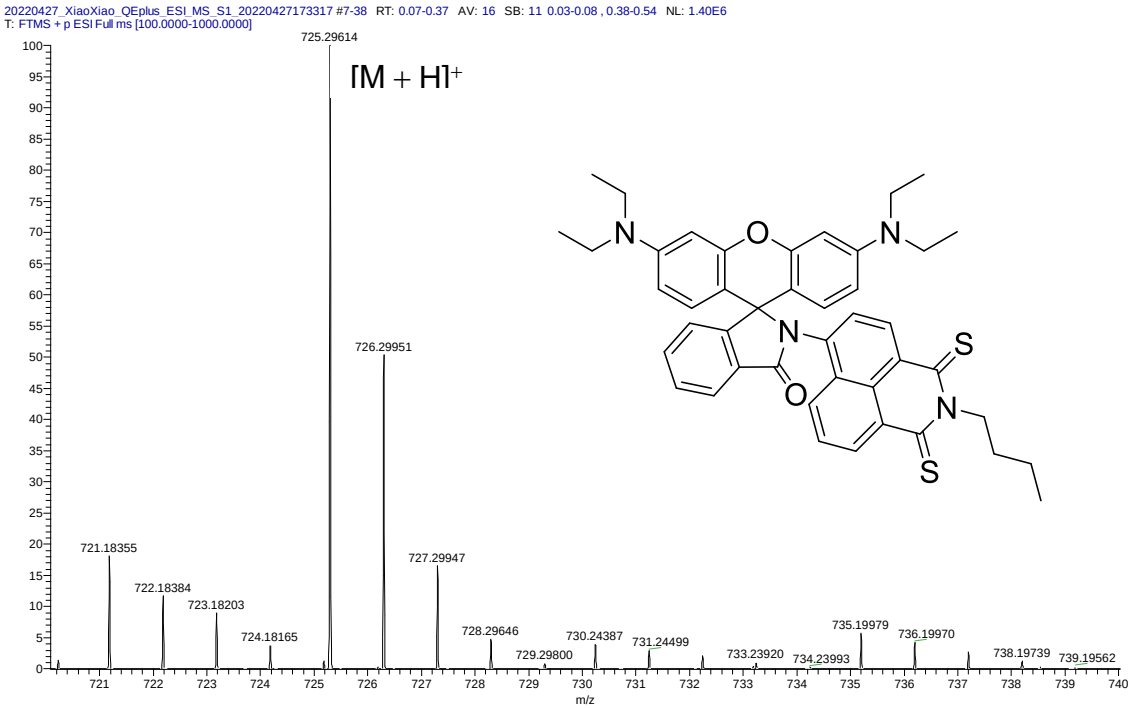

Fig. S9 ESI-HRMS of **Rho-NIS**.

3. Crystallographic Data

Table S1. Crystallographic data of **Rho-NIS** and **NIS-NHAc**

Compound	**Rho-NIS**	**NIS-NHAc**
CCDC number	2294224	2294222
Empirical formula	$C_{44}H_{44}N_4O_4S_2$	$C_{18}H_{18}N_2OS_2$
Formula weight	724.95	342.46
Colour	red	red
Temperature (K)	120	120
Wavelength (Å)	0.71073	0.71073
Crystal system	triclinic	triclinic
Space group	P-1	P-1
a (Å)	10.1465	9.2114
b (Å)	12.0918	13.4808
c (Å)	16.0775	14.5200
α (deg)	71.168	76.969
β (deg)	85.399	75.035
γ (deg)	83.566	72.648
Volume ($Å^3$)	1853.15	1640.93
Z	2	4
Dx / $g{\cdot}cm^{-3}$	1.299	1.386
F (000)	768.0	720.0
μ / mm^{-1}	0.188	0.330
Data completeness	0.997	0.998
Absorption correction	None	None
Goodness of fit on F^2	1.014	1.025
R	0.0712	0.0551
ωR_2	0.1931	0.1465

4. UV–Vis Absorption and Fluorescence Emission Spectra

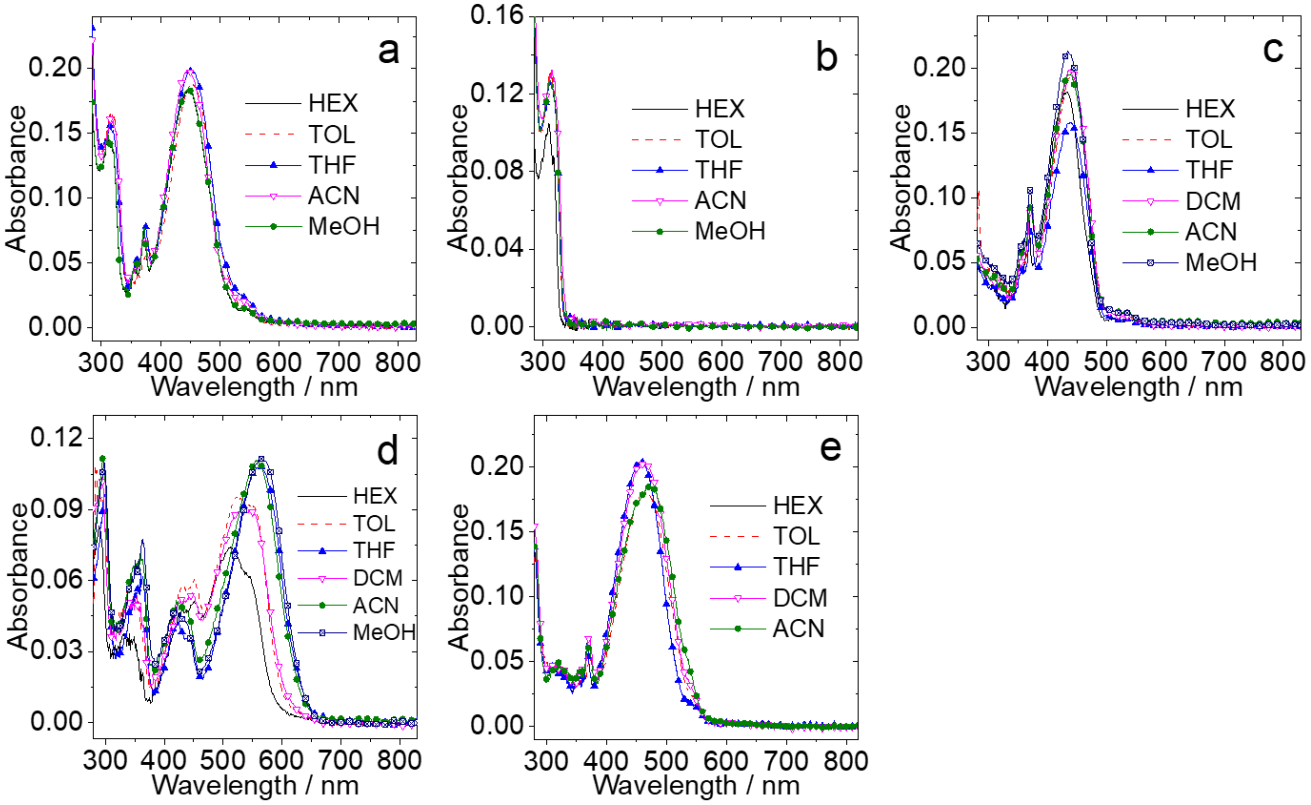

Fig. S10 UV–vis absorption spectra of the compounds (a) **Rho-NIS**, (b) **Rho**, (c) **NIS**, (d) **NIS-NH$_2$** and (e) **NIS-NHAc** in different solvents. c = 1.0 × 10^{-5} M. 25 °C.

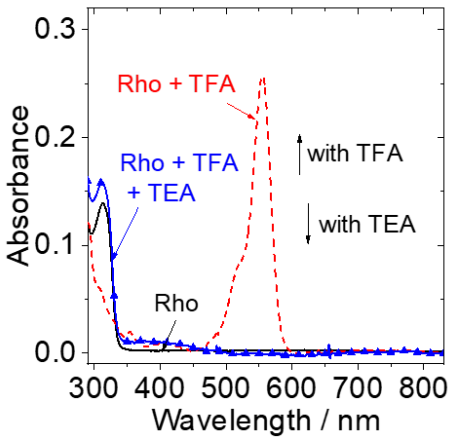

Fig. S11 UV−vis absorption spectra of **Rho** with addition of TFA (c = 40 μM) or TEA (neat, 10 μL) in MeOH. c = 1.0 × 10^{-5} M. 25 °C.

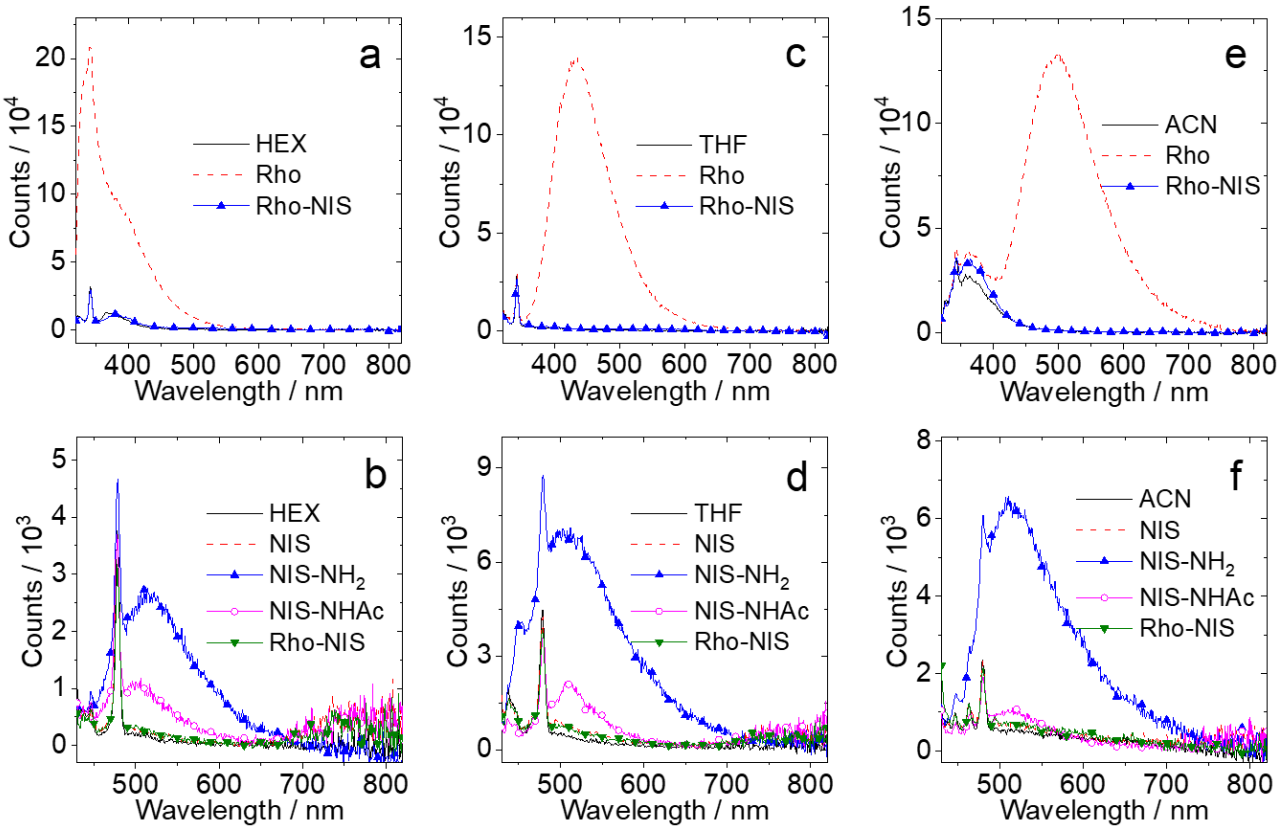

Fig. S12 Fluorescence emission spectra of the compounds in (a,b) HEX, (c,d) THF and (e,f) ACN. Top: λ_{ex} = 310 nm; Bottom: λ_{ex} = 420 nm. Optically matched solutions were used (all the solution shows the same absorbance at the excitation wavelength, A_{ex} = 0.1). ∗ stands for the Raman scattering peak of the solvent. 25 °C.

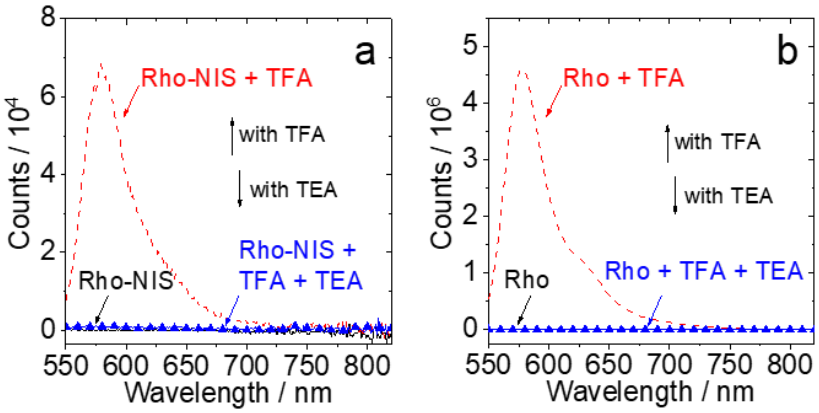

Fig. S13 Fluorescence emission spectra of (a) **Rho-NIS** in TOL and (b) **Rho** in MeOH with addition of TFA (c = 40 μM) or TEA (neat, 10 μL). λ_{ex} = 540 nm. c = 1.0 × 10^{-5} M. 25 °C.

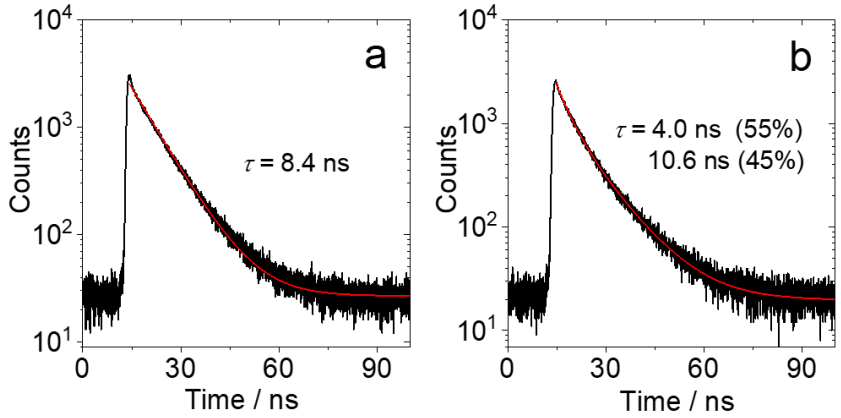

Fig. S14 Fluorescence decay traces of **NIS-NH$_2$** at 515 nm in (a) TOL and (b) ACN. λ_{ex} = 445 nm, c = 3.0 × 10^{-5} M, 25 °C.

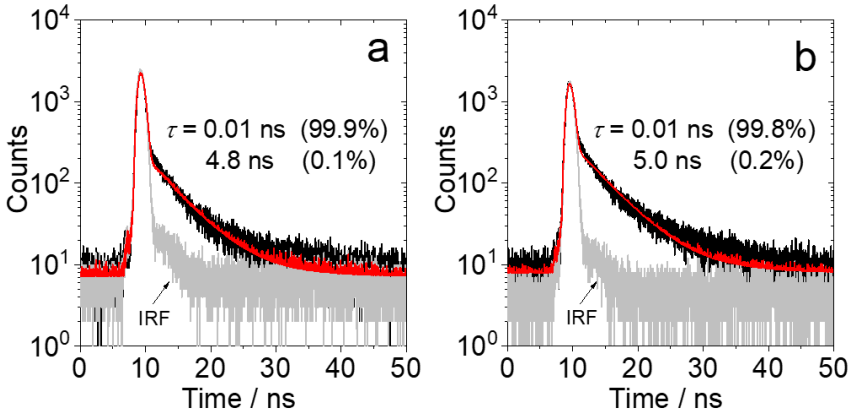

Fig. S15 Fluorescence decay traces of **NIS-NHAc** at 505 nm in (a) TOL and (b) ACN. λ_{ex} = 445 nm, c = 3.0 × 10^{-5} M, 25 °C.

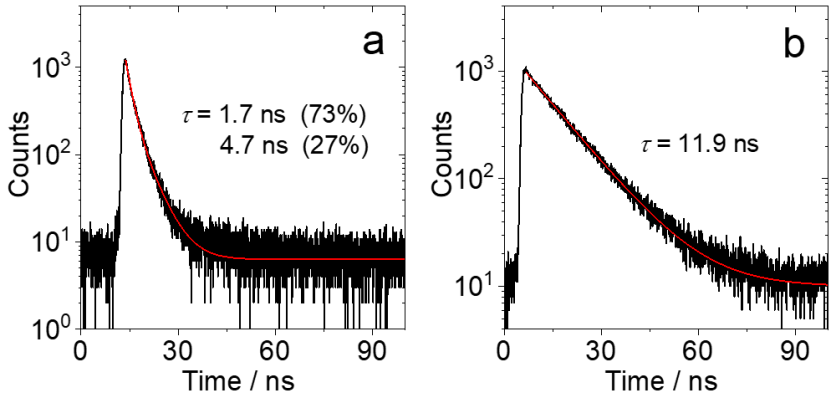

Fig. S16 Fluorescence decay traces of **Rho** (a) at 390 nm in TOL and (b) at 500 nm in ACN. λ_{ex} = 340 nm, c = 3.0 × 10^{-5} M, 25 °C.

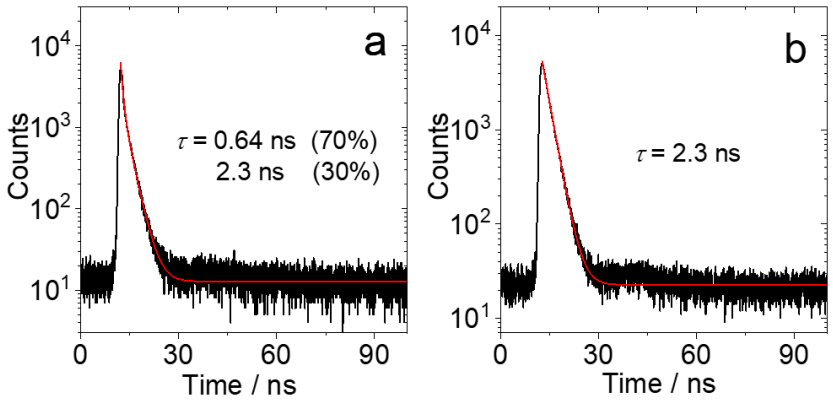

Fig. S17 Fluorescence decay traces of (a) **Rho-NIS** and (b) **Rho** at 578 nm with addition of TFA (c = 40 μM) in MeOH. λ_{ex} = 510 nm, c = 1.0 × 10^{-5} M, 25 °C.

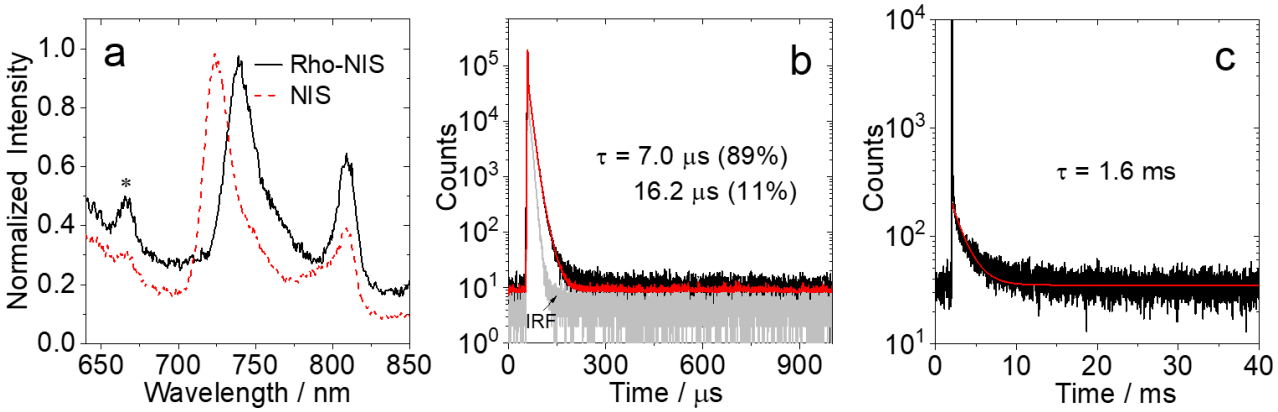

Fig. S18 (a) Normalized phosphorescence spectra of **Rho-NIS** and **NIS**. The corresponding phosphorescence decay traces of (b) **Rho-NIS** at 740 nm and (c) **NIS** at 725 nm at 77 K in MeTHF. * stands for the luminescence of MeTHF at 77 K. λ_{ex} = 445 nm, c = 1.0 × 10^{-4} M.

5. Electrochemical Studies

For the eqs (2)– (5), where ΔG_S is the static Coulombic energy, ΔG^0_{CS} is the Gibbs free-energy change of charge separation process ΔG^0_{CR} is the Gibbs free-energy change of charge recombination process and E_{CSS} is the energy levels of the charge separated state. e is the electronic charge, E_{OX} is the half-wave potential for one-electron oxidation of the electron-donor unit, E_{RED} is the half-wave potential for one-electron reduction of the electron-acceptor unit, E_{00} is the approximated energy UV – Vis absorption at the singlet excited state in HEX, ε_S is the static dielectric constant of the solvent, R_{CC} is the center-to-center separation distance between the electron donor (rhodamine) and electron acceptor (naphthalenediimide), determined by DFT optimization of the geometry, R_D is the radius of the electron donor, R_A is the radius of the electron acceptor, ε_{REF} is the static dielectric constant of the solvent used for the electrochemical studies, ε_0 is permittivity of free space. The solvents used in the calculation of free energy of the electron transfer is HEX (ε_S = 1.88), TOL (ε_S = 2.38), THF (ε_S = 7.39), DCM (ε_S = 8.93) and ACN (ε_S = 37.5).

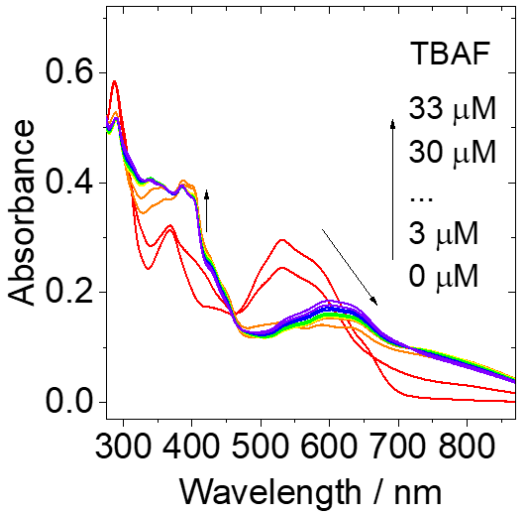

Fig. S19 UV-vis absorption spectra of **NIS-NH$_2$** chemically reduced with tetrabutylammonium fluoride (TBAF) used to generate [**NIS-NH$_2$**]$^{-\bullet}$ in deaerated DMF. c = 3.0 × 10^{-5} M. 25 °C.

6. Femtosecond Transient Absorption Spectra

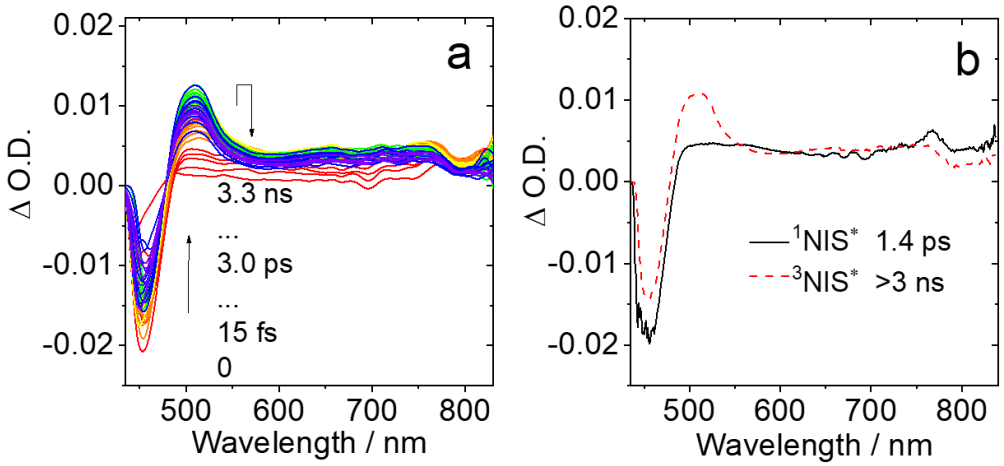

Fig. S20 (a) Femtosecond transient absorption spectra of **NIS** and (b) the related evolution associated difference spectra (EADS) of **NIS** obtained from target analysis with the sequential model in ACN. λ_{ex} = 355 nm. c = 1.0 × 10^{-4} M, 25 °C.

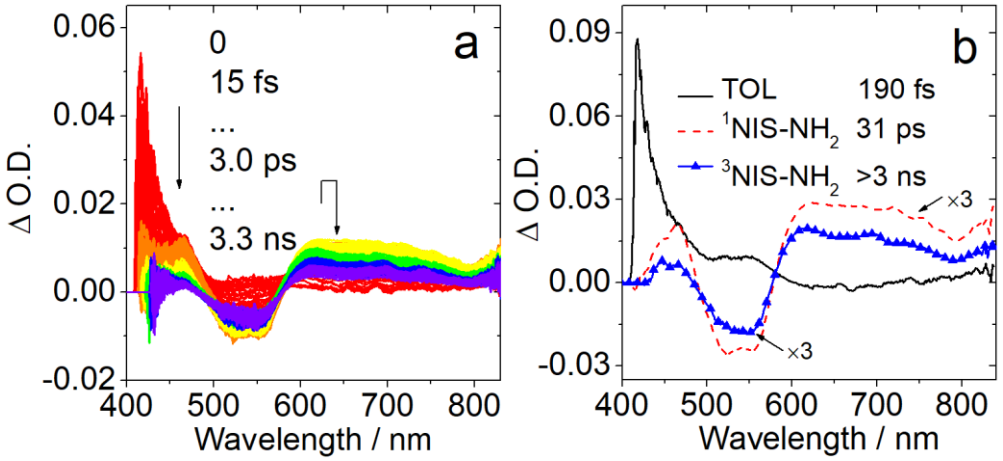

Fig. S21 (a) Femtosecond transient absorption spectra of **NIS-NH₂** and (b) the related evolution associated difference spectra (EADS) of **NIS-NH₂** obtained from target analysis with the sequential model in TOL. λ_{ex} = 355 nm. c = 1.0 × 10^{-4} M, 25 °C.

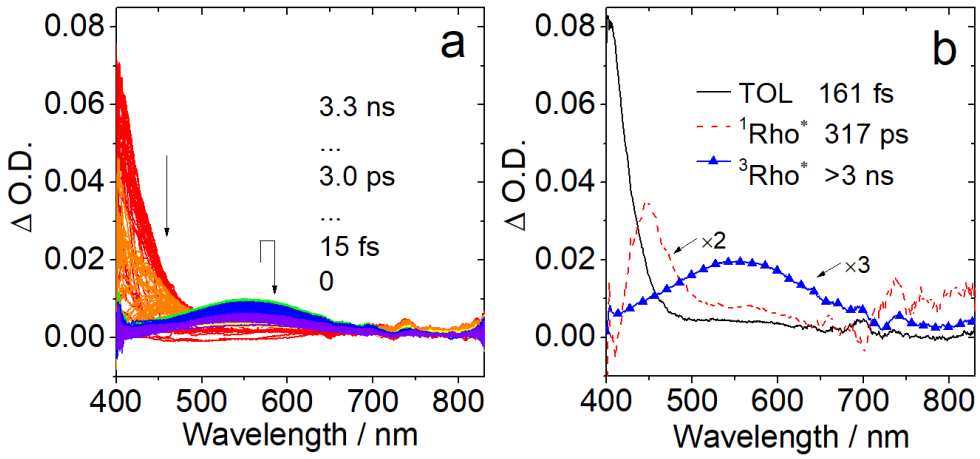

Fig. S22 (a) Femtosecond transient absorption spectra of **Rho** and (b) the related evolution associated difference spectra (EADS) of **Rho** obtained from target analysis with the sequential model in TOL. λ_{ex} = 355 nm. c = 1.0 × 10^{-4} M, 25 °C.

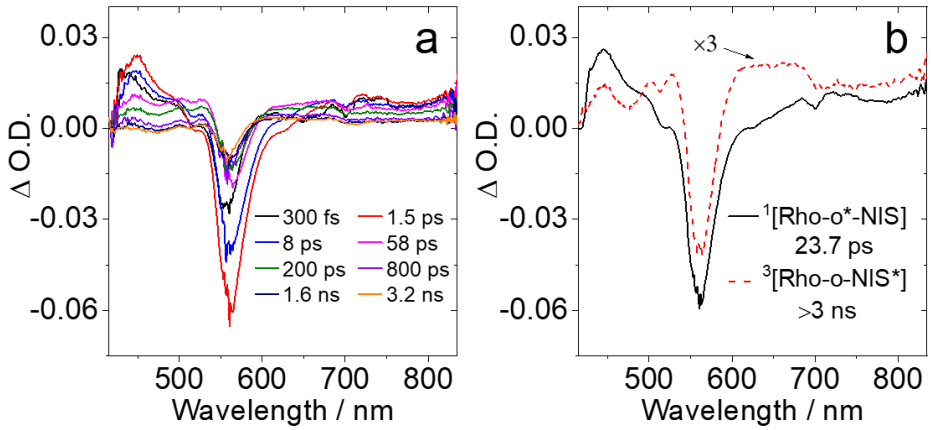

Fig. S23 (a) Femtosecond transient absorption spectra of **Rho-NIS** in the presence of TFA and (b) the related evolution associated difference spectra (EADS) obtained from target analysis with the sequential model in TOL. λ_{ex} = 355 nm. c[**Rho-NIS**] = 1.0 × 10^{-4} M, c[TFA] = 5.0 × 10^{-4} M, 25 °C.

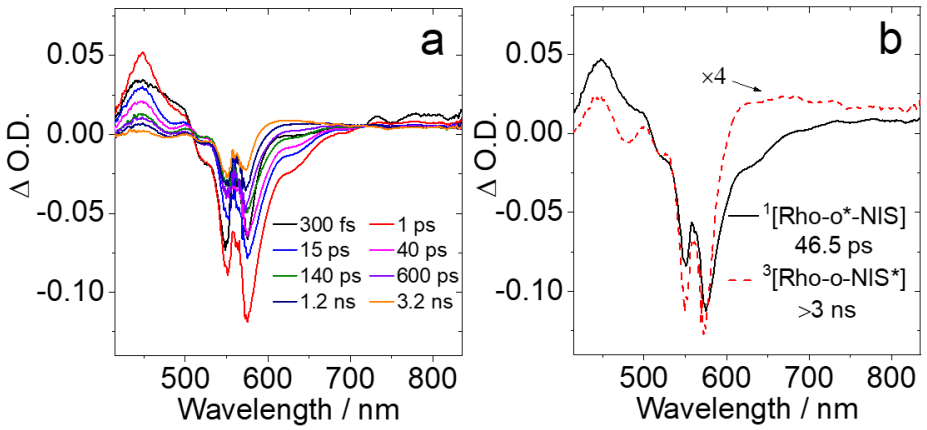

Fig. S24 (a) Femtosecond transient absorption spectra of **Rho-NIS** in the presence of TFA and (b) the related evolution associated difference spectra (EADS) obtained from target analysis with the sequential model in MeOH. λ_{ex} = 355 nm. *c*[**Rho-NIS**] = 1.0 × 10^{-4} M, *c*[TFA] = 5.0 × 10^{-4} M, 25 °C.

7. Nanosecond Transient Absorption Spectra

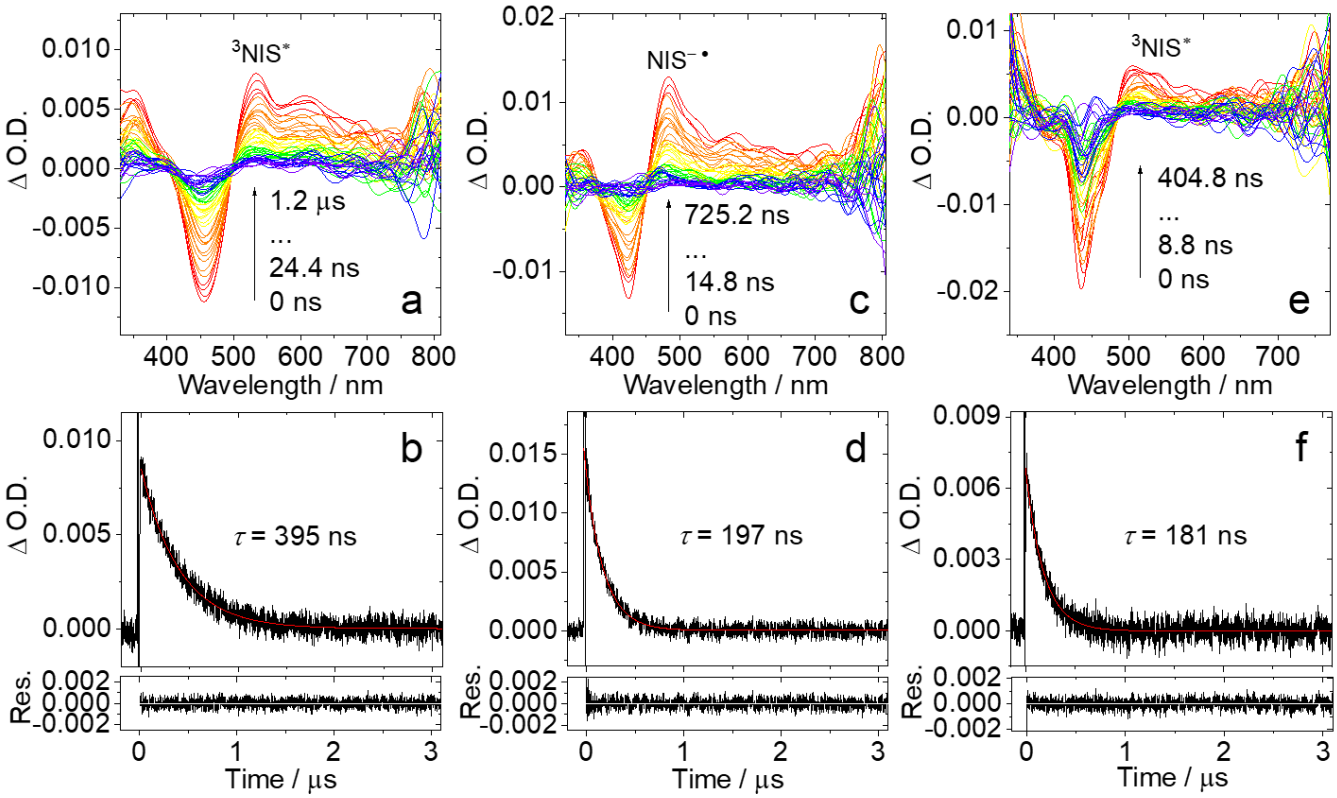

Fig. S25 Nanosecond transient absorption spectra of **Rho-NIS** in deaerated (a) TOL and (c) ACN. The decay traces of **Rho-NIS** in deaerated (b) TOL at 540 nm and (d) ACN at 480 nm excited with nanosecond pulsed laser. λ_{ex} = 420 nm. (e) Nanosecond transient absorption spectra of **NIS** and (f) the decay trace of **NIS** at 510 nm in deaerated TOL excited with nanosecond pulsed laser. λ_{ex} = 440 nm. c = 3.0 × 10^{-5} M, 25 °C.

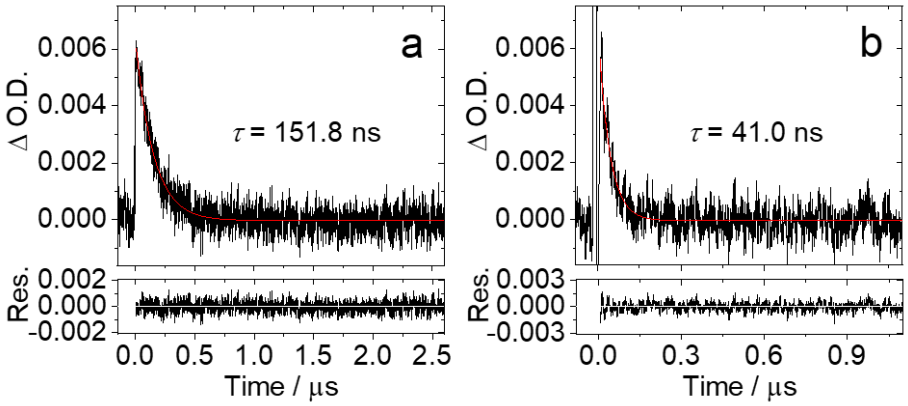

Fig. S26 The decay traces of **Rho-NIS** in aerated (a) TOL at 540 nm and (b) ACN at 480 nm excited with nanosecond pulsed laser. λ_{ex} = 440 nm. c = 3.0 × 10^{-5} M, 25 °C.

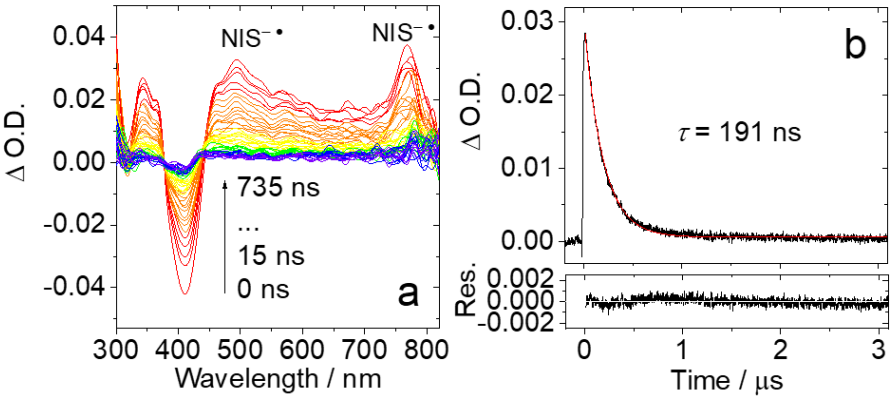

Fig. S27 (a) Nanosecond transient absorption spectra of **Rho-NIS** in deaerated MeOH and (b) the corresponding decay traces at 480 nm excited with nanosecond pulsed laser. λ_{ex} = 355 nm. c = 4.0 × 10^{-5} M.

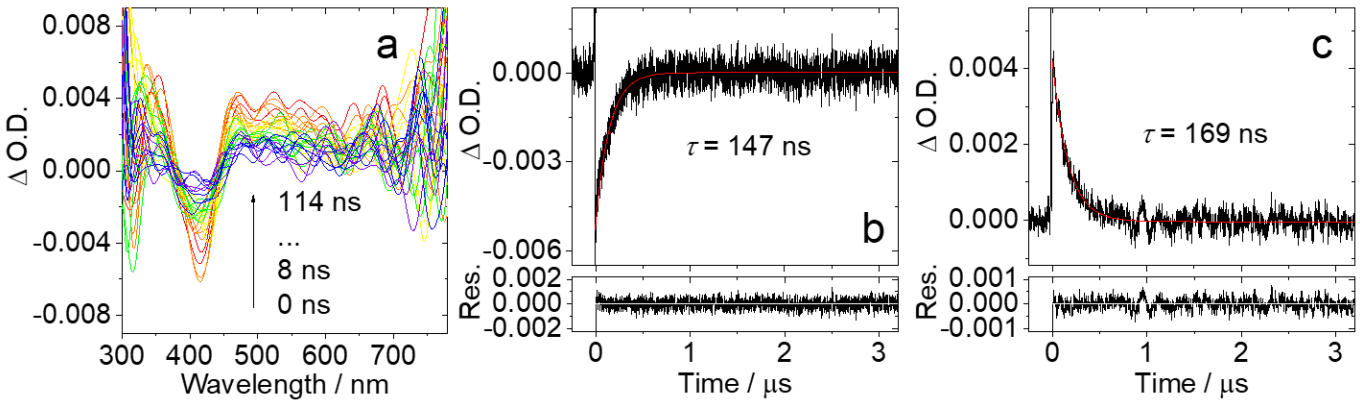

Fig. S28 (a) Nanosecond transient absorption spectra of **Rho-NIS** and the corresponding decay trace at (b) 420 nm and (c) 475 nm in deaerated MeOH excited with nanosecond pulsed laser. λ_{ex} = 440 nm. c = 3.0 × 10^{-5} M, 25 °C.

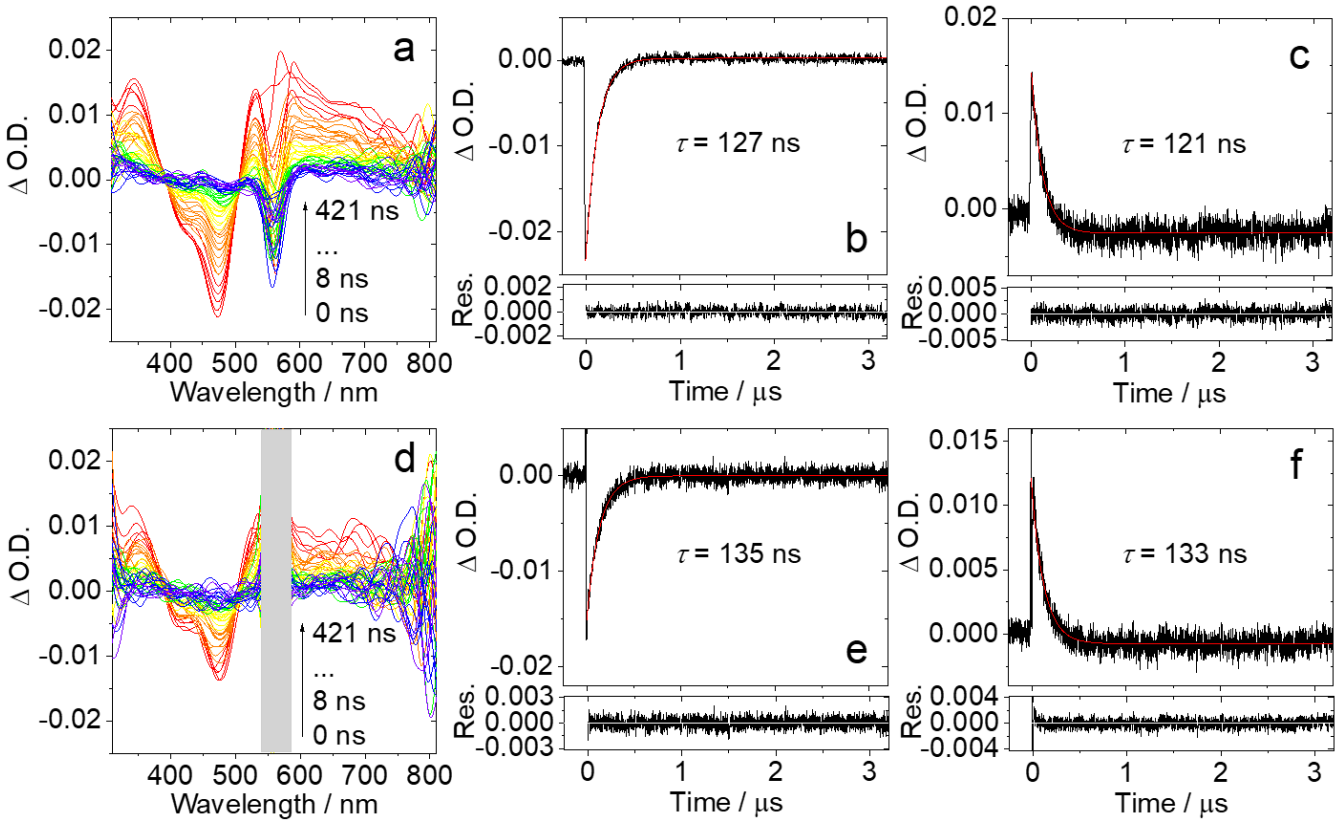

Fig. S29 (a, d) Nanosecond transient absorption spectra of **Rho-NIS** with addition of TFA (c = 40 μM) and the corresponding decay trace at (b, e) 470 nm and (c, f) 540 nm in deaerated MeOH excited with nanosecond pulsed laser. Top: λ_{ex} = 560 nm; Bottom: λ_{ex} = 450 nm. c = 1.0 × 10^{-5} M, 25 °C.

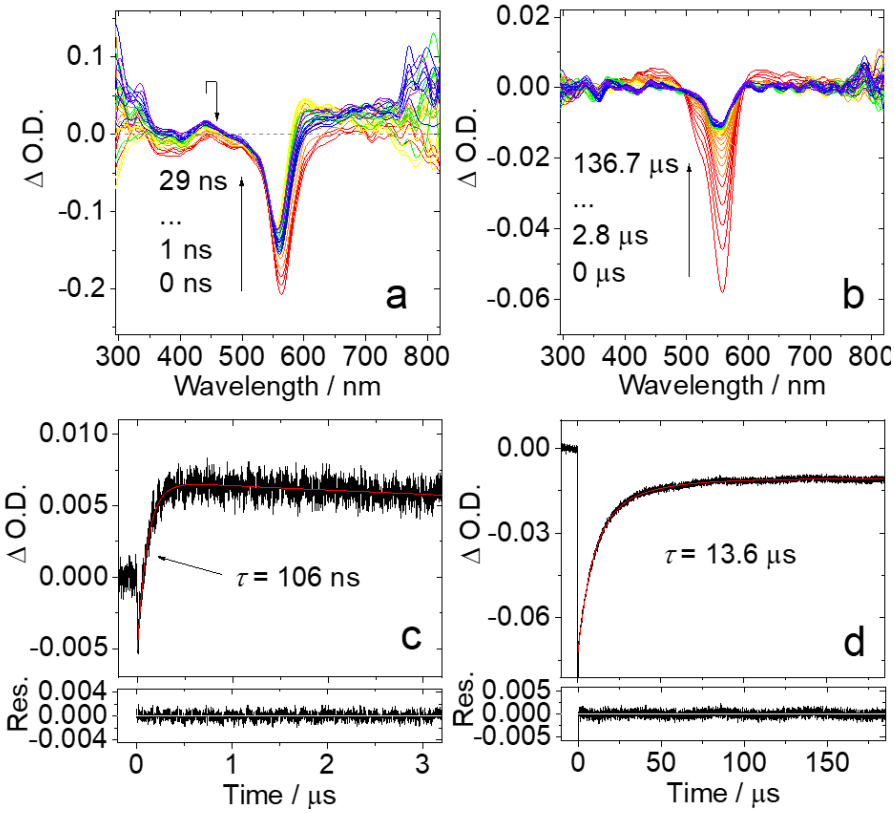

Fig. S30 Nanosecond transient absorption spectra of **Rho-NIS** with addition of TFA (c = 40 μM) in deaerated MeOH in (a) short and (b) long timescale. The corresponding decay traces at (c) 470 nm and (d) 560 nm in deaerated MeOH excited with nanosecond pulsed laser. λ_{ex} = 355 nm. c = 1.0 × 10^{-5} M. 25 °C.

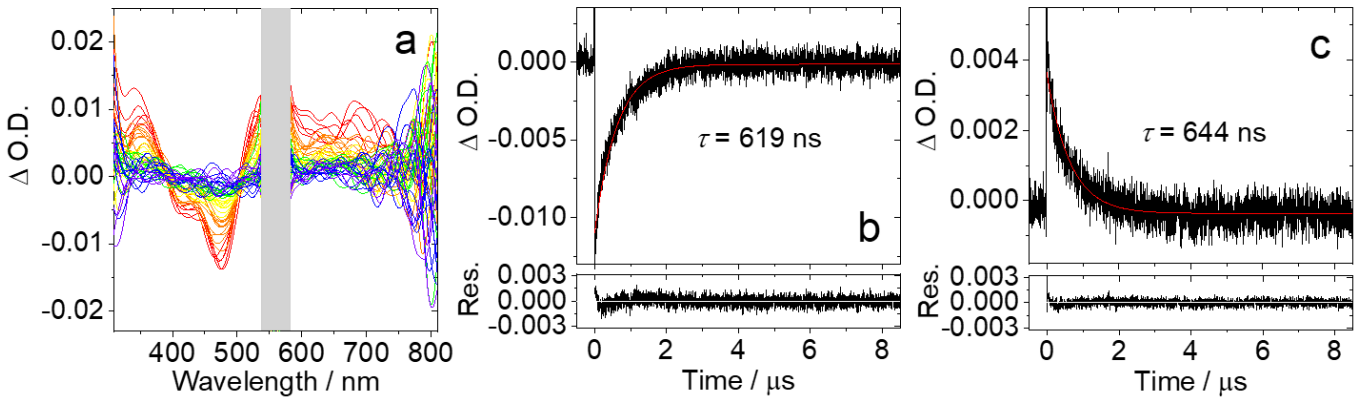

Fig. S31 (a) Nanosecond transient absorption spectra of **Rho-NIS** with addition of TFA (c = 40 μM) and the corresponding decay trace at (b) 470 nm and (c) 540 nm in deaerated TOL excited with nanosecond pulsed laser. λ_{ex} = 450 nm. c = 1.0 × 10^{-5} M, 25 °C.

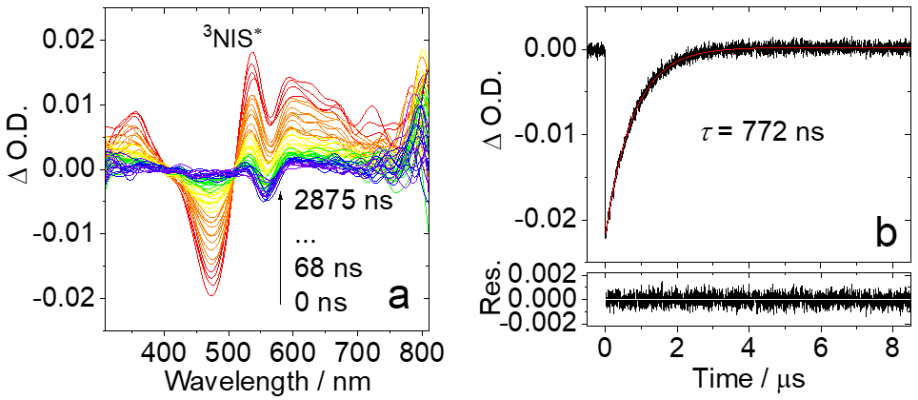

Fig. S32 (a) Nanosecond transient absorption spectra of **Rho-NIS** with addition of TFA (c = 40 μM) and (b) the corresponding decay trace at 470 nm in deaerated TOL excited with nanosecond pulsed laser. λ_{ex} = 560 nm. c = 1.0 × 10^{-5} M. 25 °C.

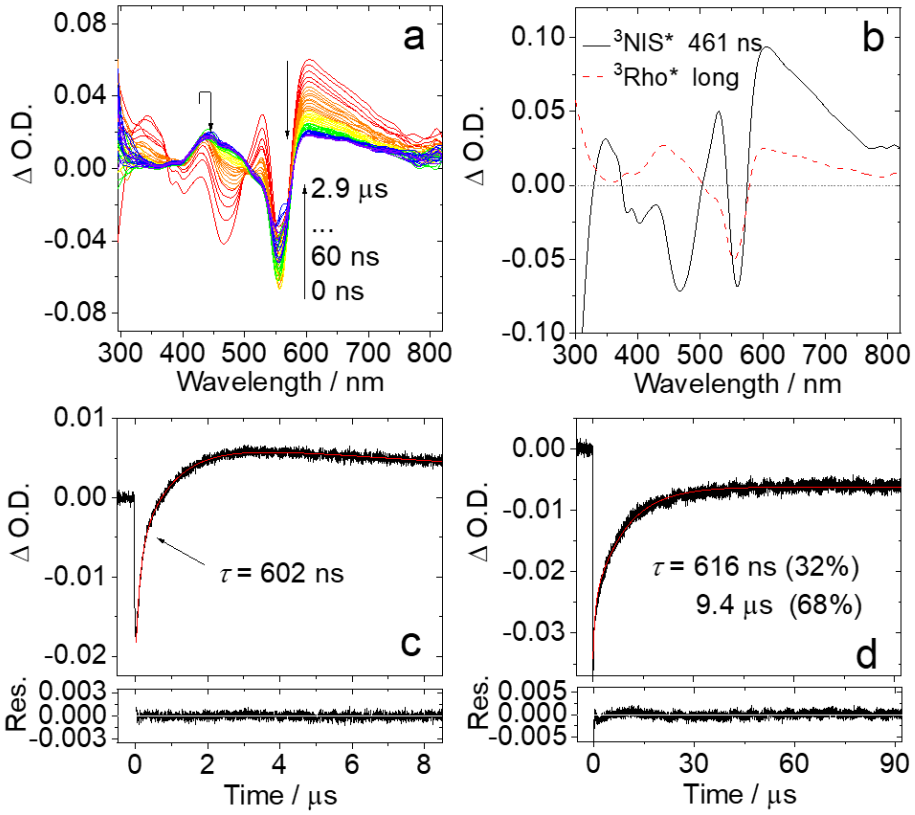

Fig. S33 (a) Nanosecond transient absorption spectra of **Rho-NIS** with addition of TFA (c = 40 μM). (b) The related evolution-associated difference spectrum (EADS) obtained from target analysis with the sequential model. And the decay traces at (c) 470 nm and (d) 560 nm in deaerated TOL excited with nanosecond pulsed laser. λ_{ex} = 355 nm. c = 1.0 × 10^{-5} M. 25 °C.

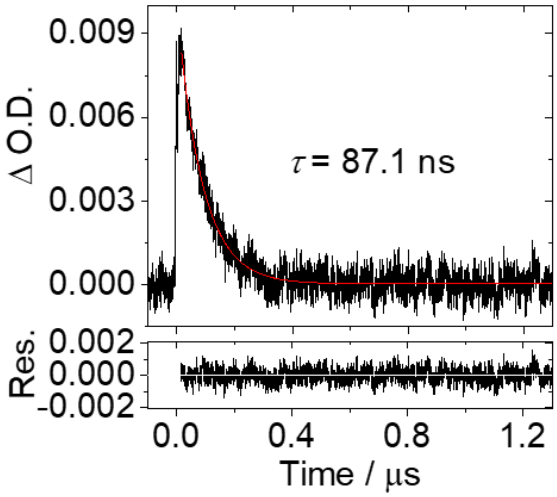

Fig. S34 The decay trace of **NIS** at 520 nm in aerated TOL excited with nanosecond pulsed laser. λ_{ex} = 355 nm. c = 4.0 × 10^{-5} M, 25 °C.

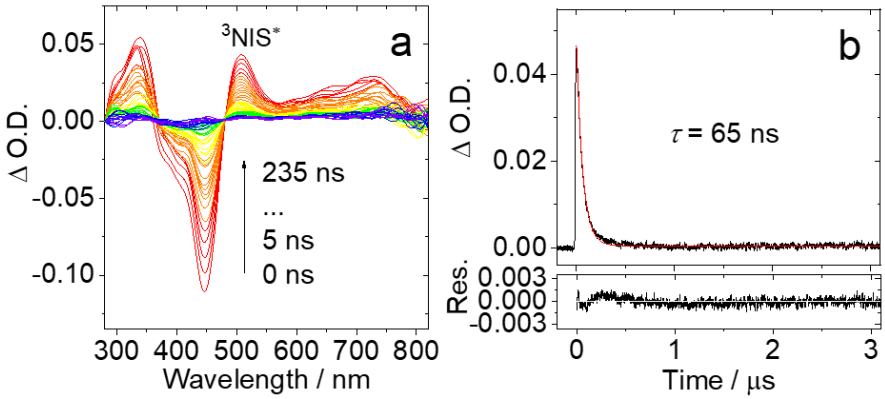

Fig. S35. (a) Nanosecond transient absorption spectra of **NIS** and (b) the decay trace of **NIS** at 520 nm in deaerated ACN excited with nanosecond pulsed laser. λ_{ex} = 355 nm. c = 4.0 × 10^{-5} M, 25 °C.

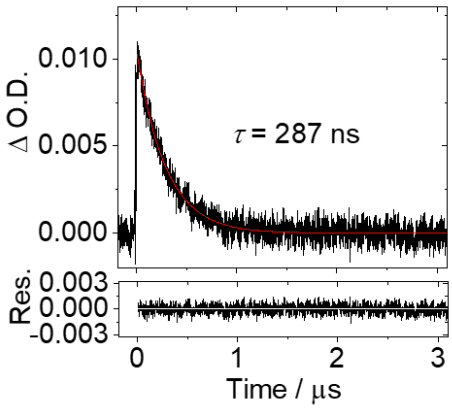

Fig. S36 The decay traces of **NIS-NH$_2$** in aerated TOL at 630 nm excited with nanosecond pulsed laser. λ_{ex} = 530 nm. c = 2.0 × 10^{-5} M, 25 °C.

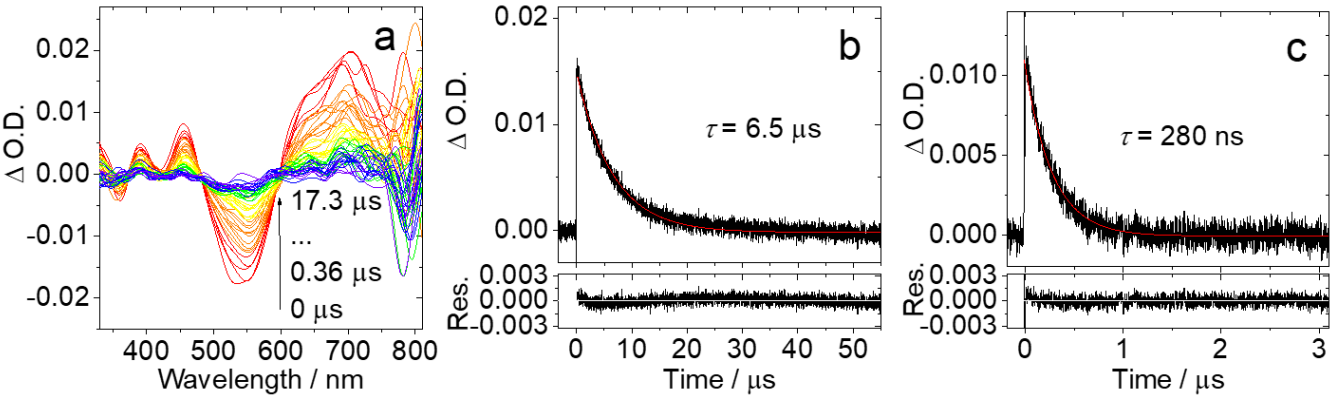

Fig. S37 (a) Nanosecond transient absorption spectra of **NIS-NH$_2$** in deaerated ACN. The decay traces of **NIS-NH$_2$** in (b) deaerated and (c) aerated ACN at 630 nm excited with nanosecond pulsed laser. λ_{ex} = 530 nm. c = 2.0 × 10^{-5} M, 25 °C.

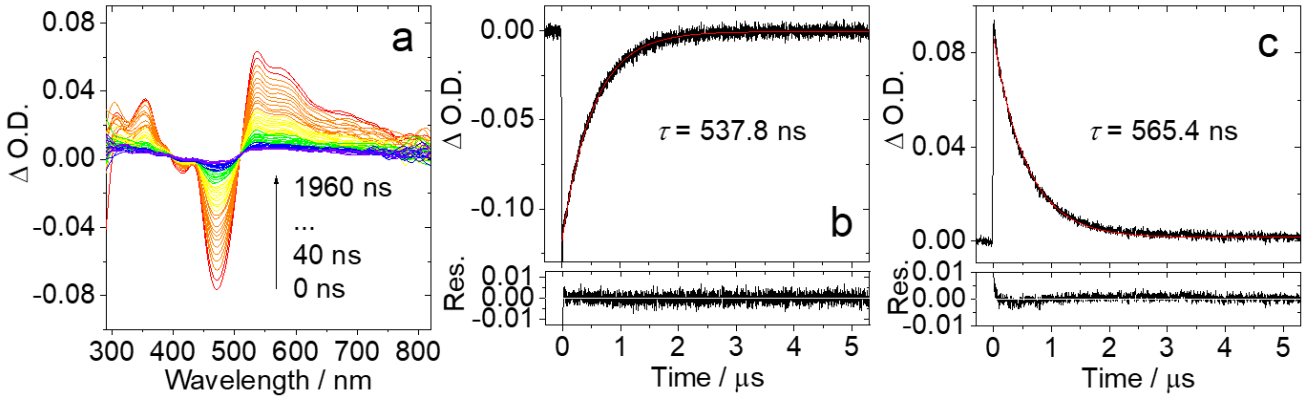

Fig. S38 (a) Nanosecond transient absorption spectra of **NIS-NHAc** in deaerated TOL. The decay traces of **NIS-NHAc** at (b) 470 nm and (c) 530 nm in deaerated TOL excited with nanosecond pulsed laser. λ_{ex} = 355 nm. c = 3.0 × 10^{-5} M, 25 °C.

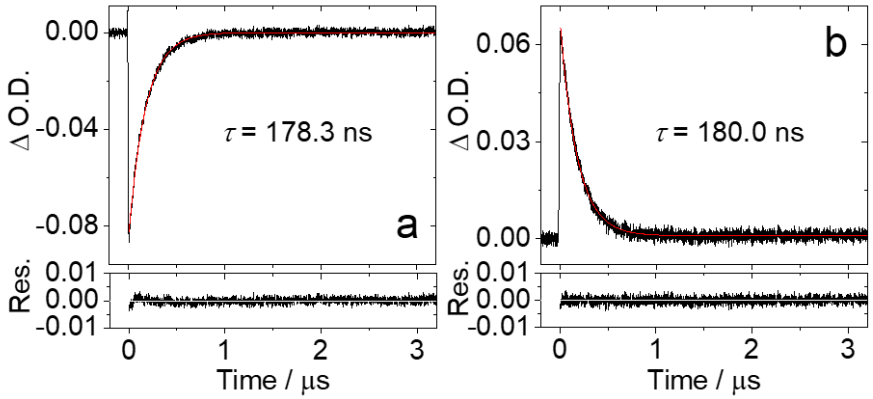

Fig. S39 The decay traces of **NIS-NHAc** at (b) 470 nm and (c) 530 nm in aerated TOL excited with nanosecond pulsed laser. λ_{ex} = 355 nm. c = 3.0 × 10^{-5} M, 25 °C.

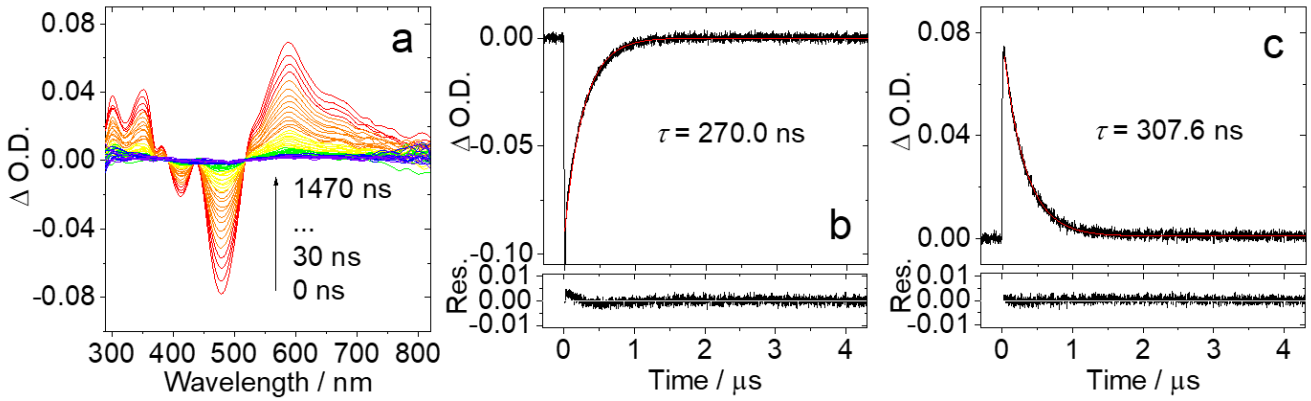

Fig. S40 (a) Nanosecond transient absorption spectra of **NIS-NHAc** in deaerated ACN. The decay traces of **NIS-NHAc** at (b) 470 nm and (c) 590 nm in deaerated ACN excited with nanosecond pulsed laser. λ_{ex} = 355 nm. c = 3.0 × 10^{-5} M, 25 °C.

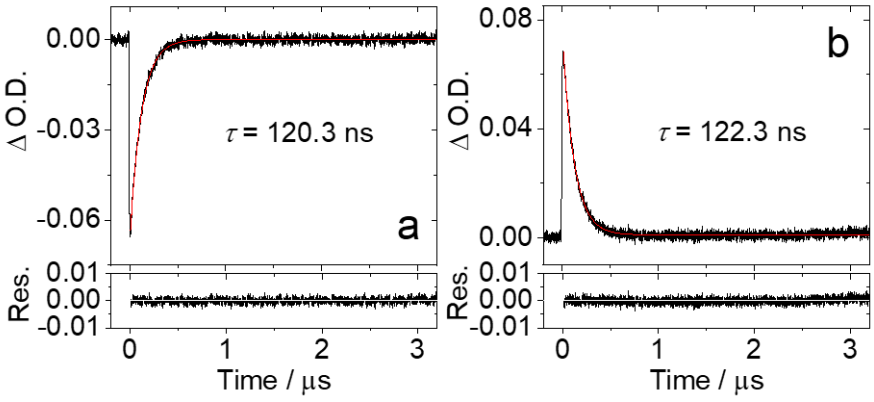

Fig. S41 The decay traces of **NIS-NHAc** at (b) 470 nm and (c) 590 nm in aerated ACN excited with nanosecond pulsed laser. λ_{ex} = 355 nm. c = 3.0 × 10^{-5} M, 25 °C.

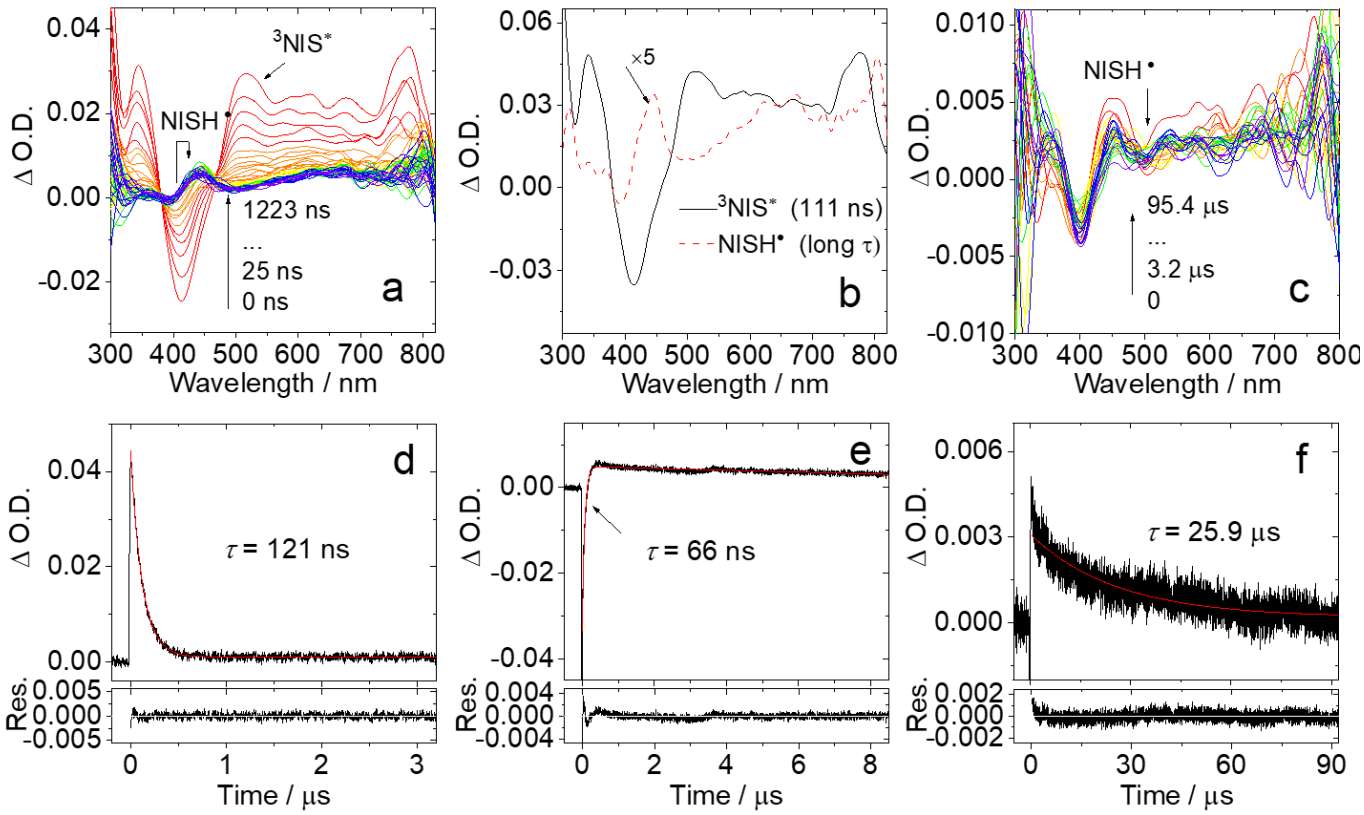

Fig. S42 Nanosecond transient absorption spectra of **Rho-NIS** in deaerated isopropanol in (a) short and (c) long timescale. (b) The related species-associated difference spectrum (SADS) obtained from target analysis with the sequential model for NIS. (d) The decay traces of **Rho-NIS** at 520 nm, and the decay traces at 440 nm in (e) short and (f) long timescale, excited with nanosecond pulsed laser. λ_{ex} = 355 nm. $c = 3.0 \times 10^{-5}$ M, 25 °C.

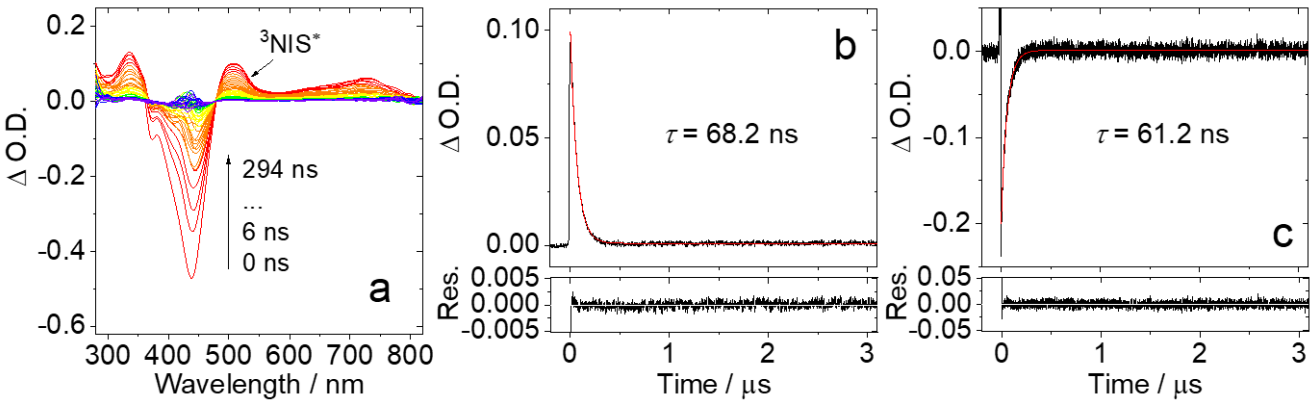

Fig. S43 (a) Nanosecond transient absorption spectra of **NIS** in aerated isopropanol. (d) The decay traces of **NIS** at (b) 520 nm and (c) 440 nm excited with nanosecond pulsed laser. λ_{ex} = 355 nm. c = 4.0 × 10^{-5} M, 25 °C.

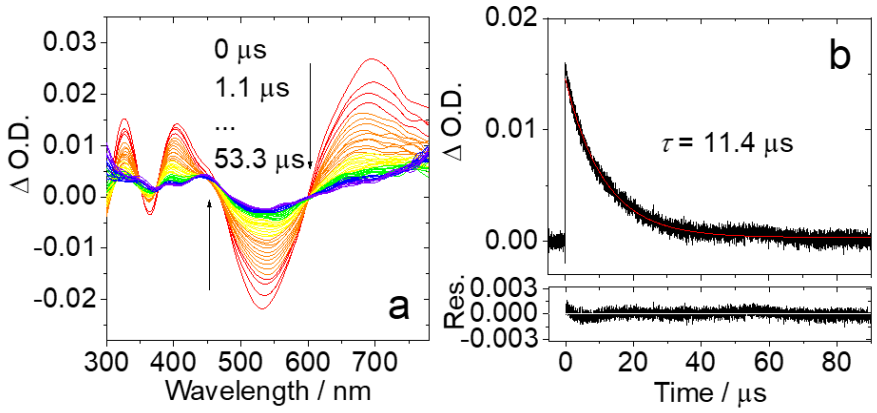

Fig. S44 (a) Nanosecond transient absorption spectra of **NIS-NH₂** and (d) the corresponding decay trace at 690 nm in deaerated isopropanol excited with nanosecond pulsed laser. λ_{ex} = 355 nm. c = 3.0 × 10^{-5} M, 25 °C.

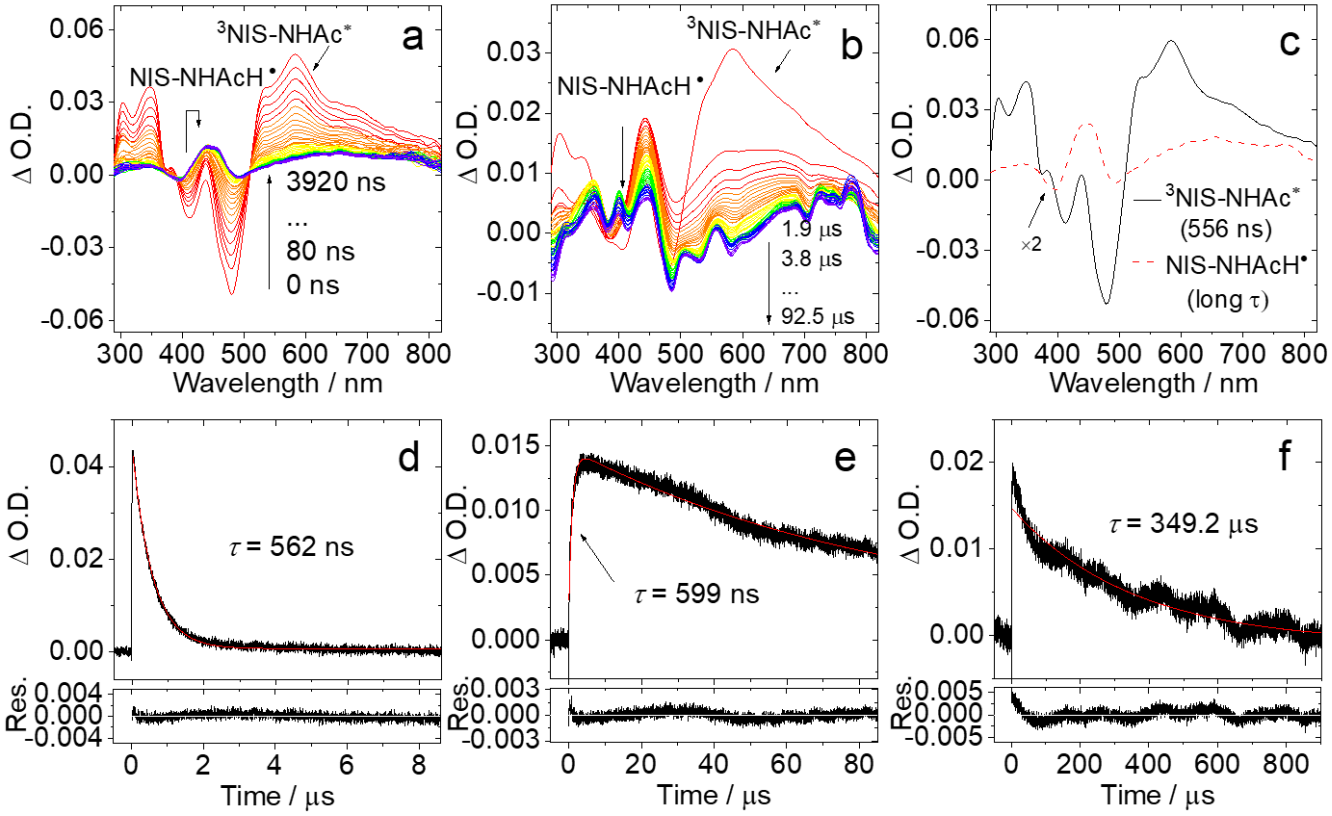

Fig. S45 Nanosecond transient absorption spectra of **NIS-NHAc** in deaerated isopropanol in (a) short and (c) long timescale. (b) The related species-associated difference spectrum (SADS) obtained from target analysis with the sequential model for NIS. (d) The decay traces of **NIS-NHAc** at 530 nm, and the decay traces at 440 nm in (e) short and (f) long timescale, excited with nanosecond pulsed laser. λ_{ex} = 355 nm. c = 3.0 × 10^{-5} M, 25 °C.

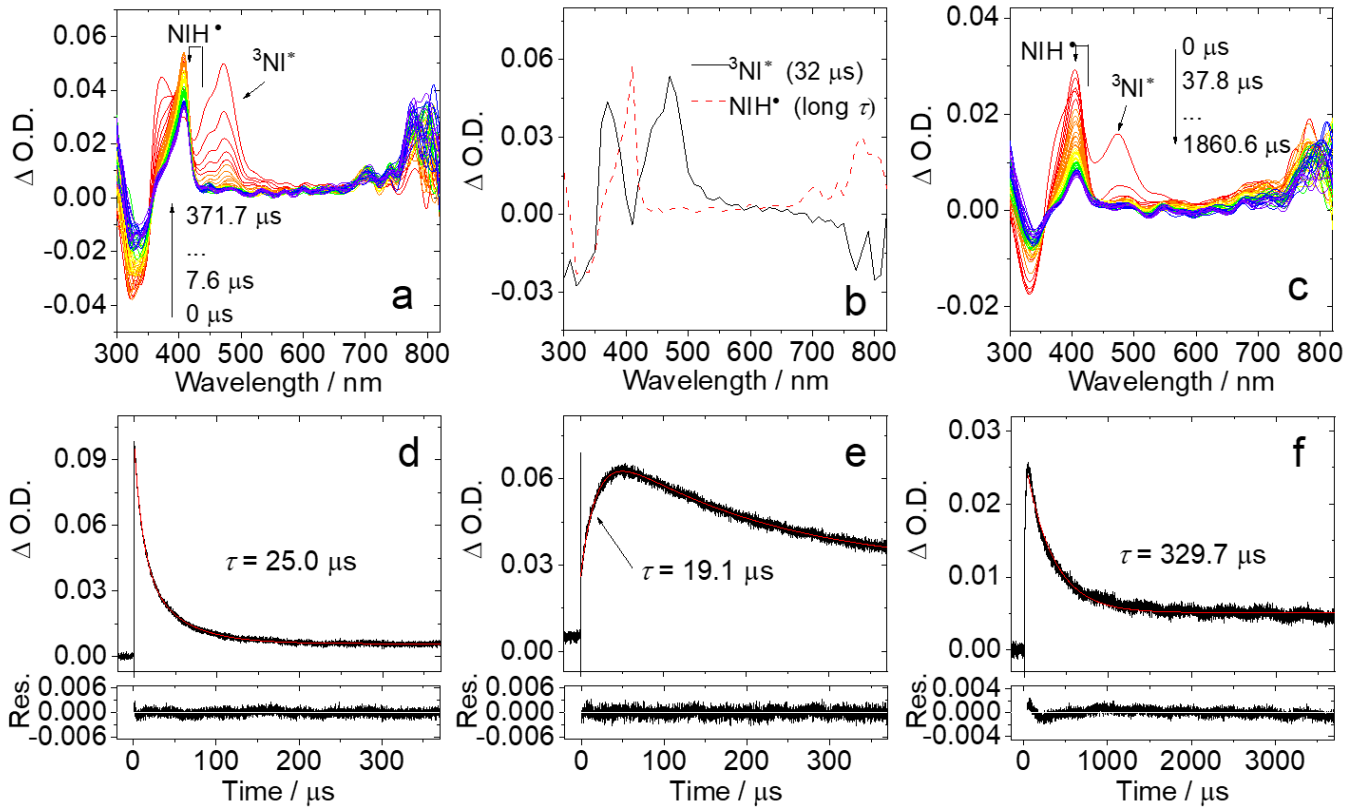

Fig. S46 Nanosecond transient absorption spectra of **NI** in deaerated isopropanol in (a) short and (c) long timescale. (b) The related species-associated difference spectrum (SADS) obtained from target analysis with the sequential model for NIS. (d) The decay traces of **NI** at 460 nm, and the decay traces at 410 nm in (e) short and (f) long timescale, excited with nanosecond pulsed laser. λ_{ex} = 355 nm. c = 3.0×10^{-5} M, 25 °C.

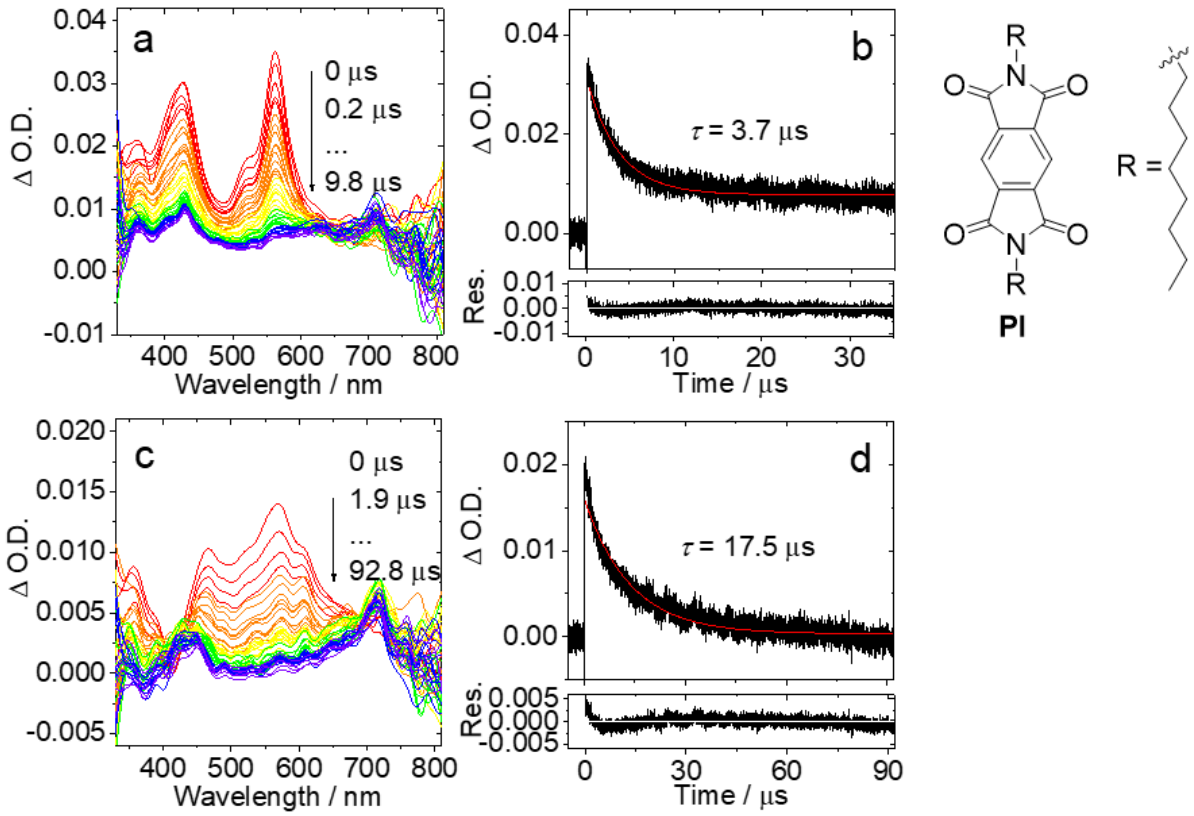

Fig. S47 Intermolecular triplet-triplet energy transfer (TTET) with pyromellitimide (**PI**) as the triplet energy donor and **4** as the triplet energy acceptor. (a) Nanosecond transient absorption spectra of **PI** and (b) the decay trace of at 430 nm in deaerated TOL. (c) Nanosecond transient absorption spectra of the mixture of **PI** (c = 1 × 10^{-4} M) and **4** (c = 5 × 10^{-5} M), and (d) decay trace of the mixture at 570 nm in deaerated TOL. λ_{ex} = 355 nm. 25 °C.

8. Charge Transfer Quantum Yield

The charge transfer quantum yield was calculated with equation S1:

$$\Phi_{CS} = \Phi_{std}\left(\frac{\Delta O.D._{\cdot sam}}{\Delta O.D._{\cdot std}}\right)\left(\frac{\varepsilon_{std}}{\varepsilon_{sam}}\right) \quad (S1)$$

Where Φ_{std} is the triplet state quantum yield of the standard compound; $\Delta O.D._{\cdot sam}$ and $\Delta O.D._{\cdot std}$ are the $\Delta O.D.$ value of the sample' s radical anion/cation and the standard compound' s excited state at the maximal absorption in transient absorption spectra, respectively (with the fact that the sample' s radical anion/cation and the standard compound' s excited state does not overlap with the ground state bleaching band as the criterion); ε_{sam} and ε_{std} are the molar absorption coefficient of the sample' s radical anion/cation and the standard compound' s excited state. It should be noted that the absorption of the sample and the standard compound at the excited wavelength should be kept same. Anthracene was selected as standard compound, the Φ_{std} and ε_{std} at 432 nm of the triplet state of anthracene is 71% and 4.55×10^4 M^{-1} cm^{-1}, respectively; ε_{std}, i.e. the molar absorption coefficient at 418 nm of the **NIS** radical anion, is 9.50×10^3 M^{-1} cm^{-1}; the molar absorption coefficient at 418 nm of the NI radical anion, is 2.75×10^4 M^{-1} cm^{-1}.[5] The excitation wavelength is 355 nm and the absorbance of the sample and the anthracene is 0.18 at 355 nm.

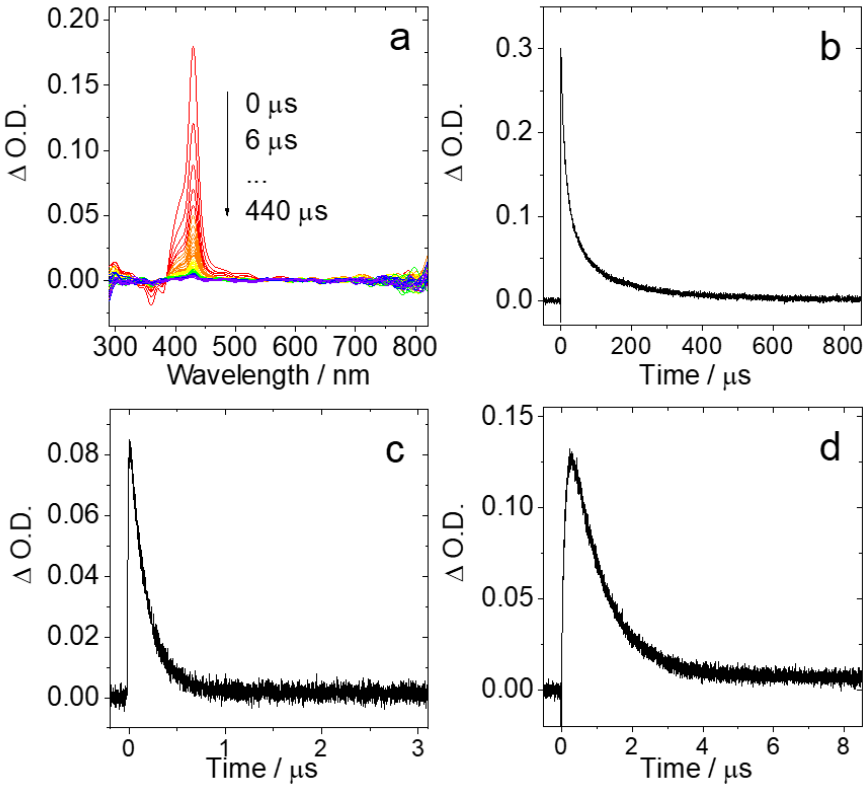

Fig. S48 (a) Nanosecond transient absorption spectra of anthracene and (b) the decay trace at 432 nm in deaerated TOL. The decay traces of (c) **Rho-NIS** in deaerated ACN at 480 nm and (d) **Rho-NI** in deaerated HEX at 418 nm excited with nanosecond pulsed laser. $\lambda_{ex} = 355$ nm. A = 0.18 at 355 nm, 20 °C.

9. Time-Resolved Electron Paramagnetic Resonance (TREPR) Spectra

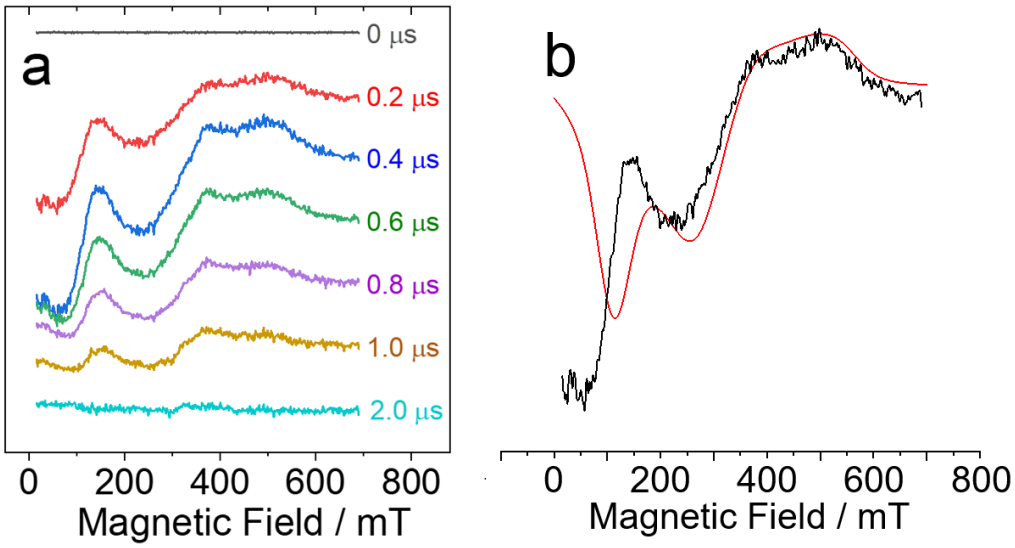

Fig. S49 TREPR spectra of **NIS-NH$_2$** measured with X-band spectrometer excited with 450 nm laser with energy 1 mJ per pulse (a) at different delay time and (b) at 0.2 μs in TOL/2-MeTHF (1:3, v/v) at 80 K. Simulation (red curve in b) was performed with EasySpin package. Simulation parameters are the same as for simulation spectrum in Q-band. $c = 1.0 \times 10^{-4}$ M.

The forbidden transition of **NIS-NH$_2$** is observed in weak fields of the TREPR spectrum in the X-band. The width, intensity and position of the theoretical spectrum differs from the experimental one. Agreement can be improved by increasing the width of this signal, or by assuming that the narrow signal is superimposed on the wide signal in the null fields.

10. DFT Calculations

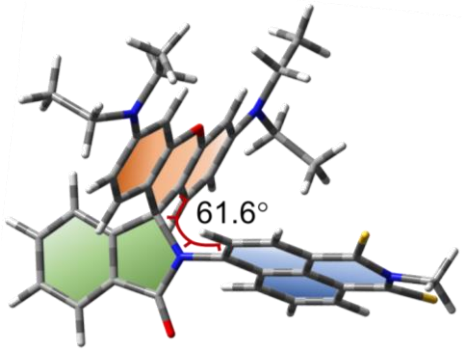

Fig. S50 Optimized ground state geometry of **Rho-NIS**. The selected dihedral angles are presented. Calculations were performed by DFT at the B3LYP/6-31G(d) level with Gaussian 09.

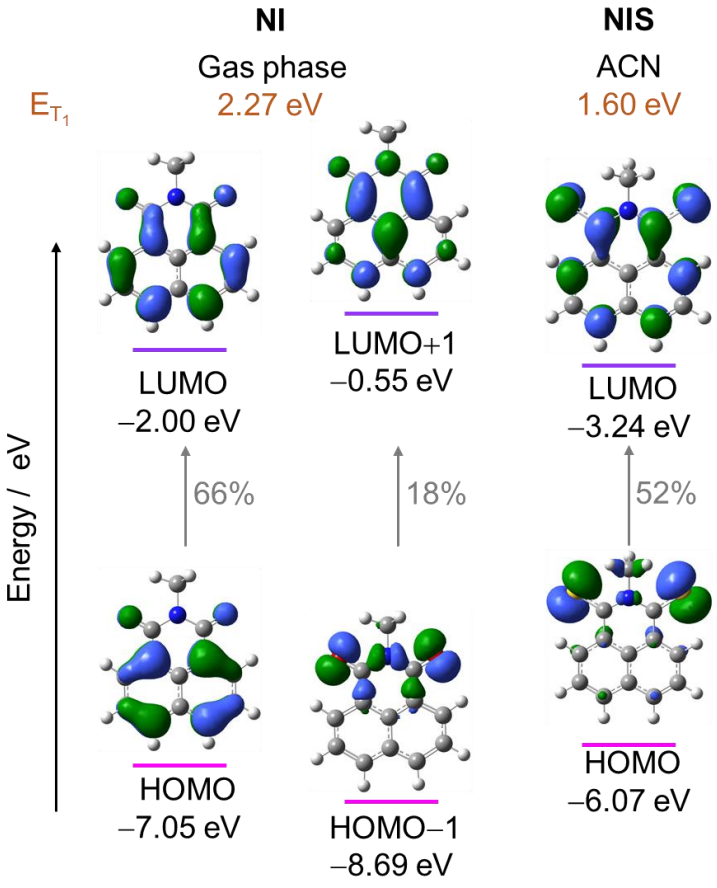

Fig. S51 Selected frontier molecular orbitals taking part in the T_1 states of **NI** in gas phase and **NIS** in ACN (isovalue = 0.04). The orbital transition probability and energy of T_1 states are also shown. Calculation was performed by DFT at the UB3LYP/6-31G(d) level with Gaussian 09.

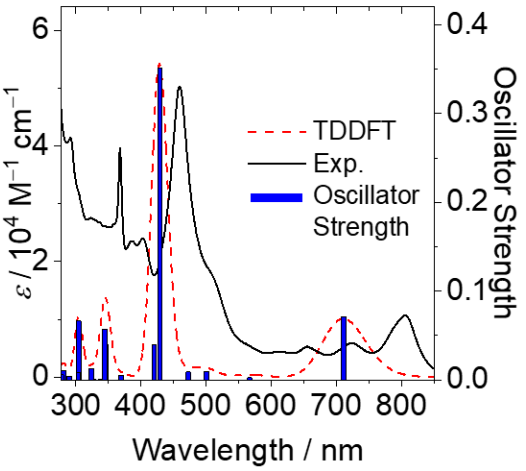

Fig. S52 Comparison of calculation and experimental data of UV-vis spectra for $NIS^{-\bullet}$ of **NIS**. The calculations are performed by TDDFT at the UB3LYP/6-31G(d) level with Gaussian 09 in ACN. The experimental data were measured by chemical redox.

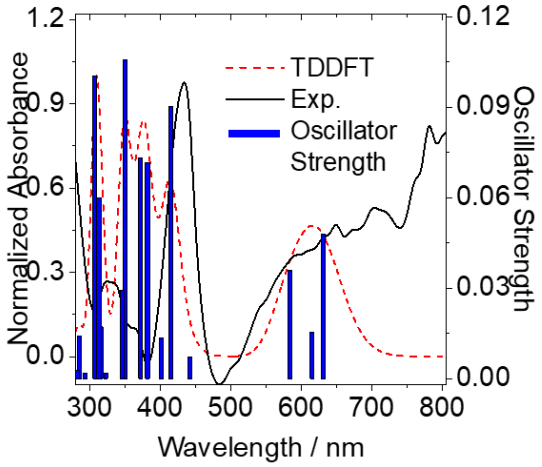

Fig. S53 Comparison of calculation and experimental data of UV-vis spectra for $NISH^{\bullet}$. The calculations are performed by TDDFT at the UB3LYP/6-31G(d) level with Gaussian 09 in ACN. The experimental data were obtained by nanosecond transient absorption spectra of NIS in deaerated isopropanol.

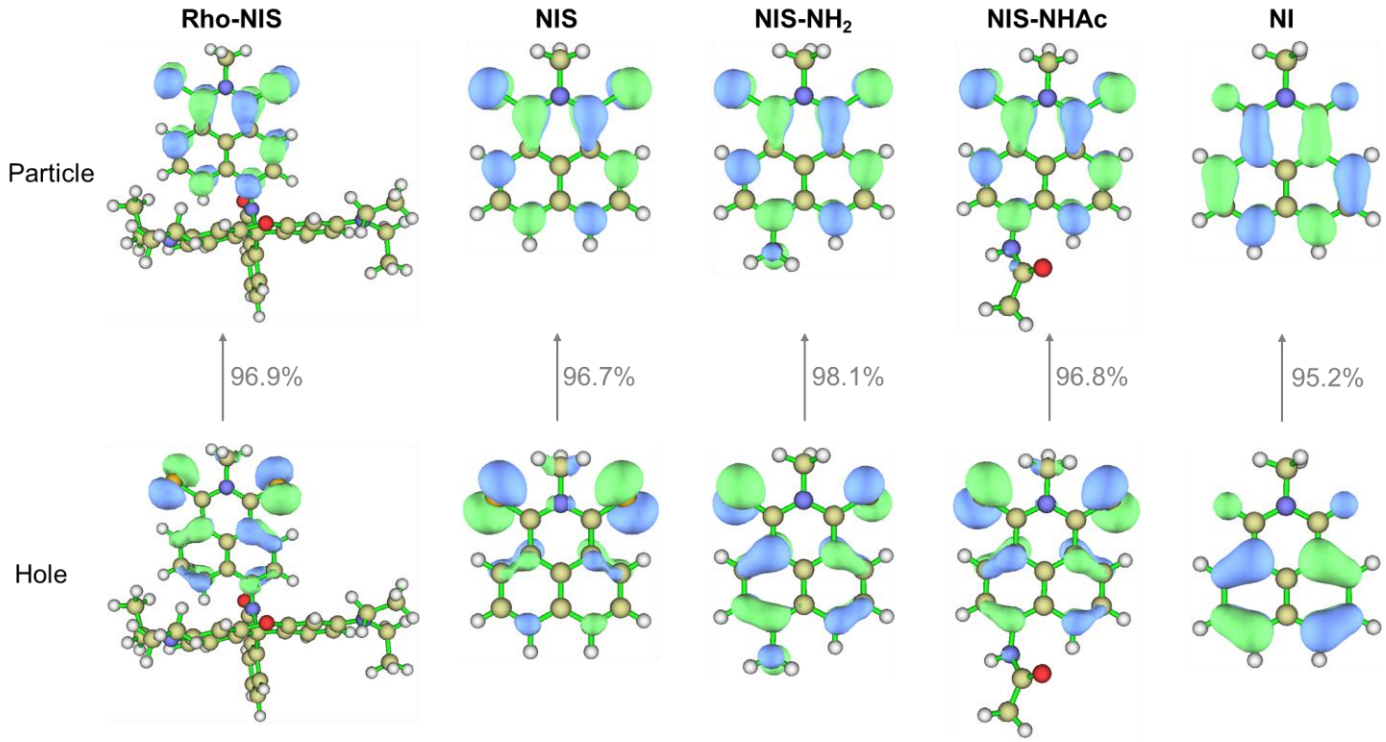

Fig. S54 The natural transition orbital (NTO) pairs taking part in the T_1 states of the compounds (isovalue = 0.04) and their contribution to this transition in gas phase. Calculation was performed by DFT based on the optimized ground state geometry at the B3LYP/6-31G(d) level with Gaussian 09. NTO analysis was performed by Multiwfn program.

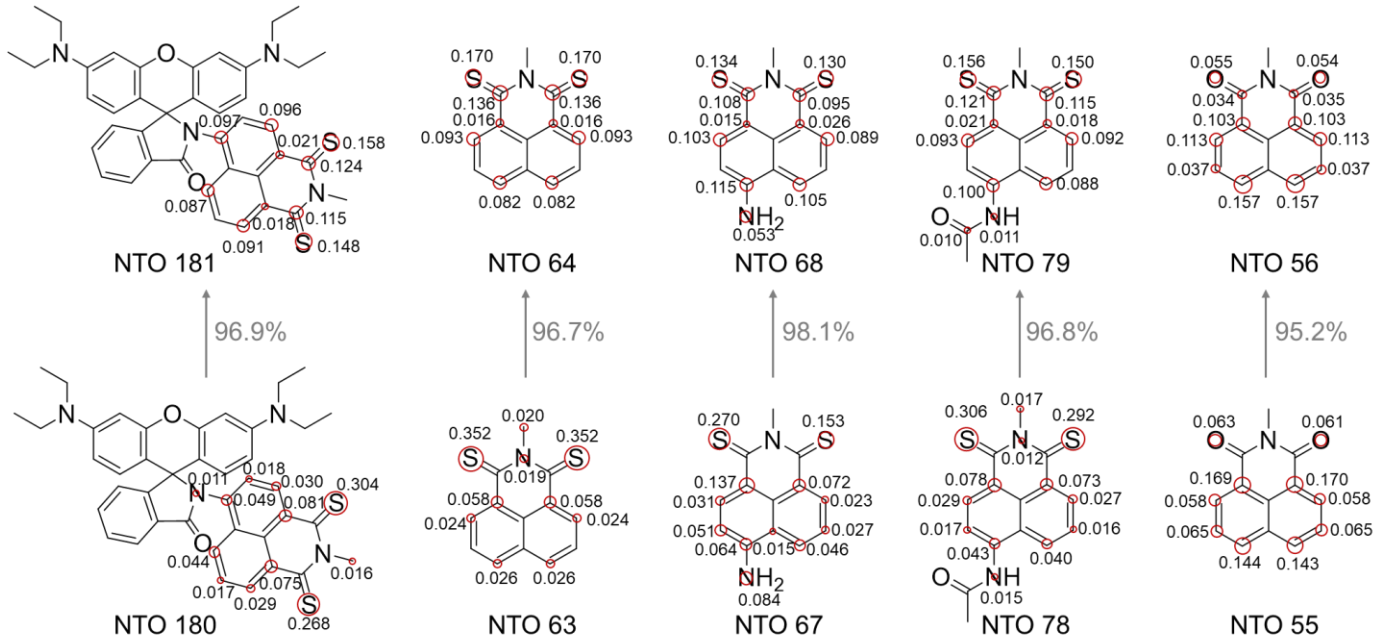

Fig. S55 The contribution of the each atom to the total NTO pairs taking part in the T_1 states of the compounds (the contribution less than 0.01 are omitted for clarity) in gas phase.

11. References

1. Y. Zhao, K. Chen, E. A. Yildiz, S. Li, Y. Hou, X. Zhang, Z. Wang, J. Zhao, A. Barbon, H. G. Yaglioglu and H. Wu, *Chem. –Eur. J.*, 2020, **26**, 3591–3599.
2. V.-N. Nguyen, S. J. Park, S. Qi, J. Ha, S. Heo, Y. Yim, G. Baek, C. S. Lim, D. J. Lee, H. M. Kim and J. Yoon, *Chem. Commun.*, 2020, **56**, 11489–11492.
3. X. Chen, A. A. Sukhanov, Y. Yan, D. Bese, C. Bese, J. Zhao, V. K. Voronkova, A. Barbon and H. G. Yaglioglu, *Angew. Chem., Int. Ed.*, 2022, e202203758.